OPTICAL PROPERTIES OF SELF-ORGANIZED SILVER NANO-ISLAND THIN FILM

by

I-Hung Ting

B.S. in Physics, National Cheng Kung University, 2009

Submitted to the Graduate Faculty of

The Swanson School of Engineering in partial fulfillment

of the requirements for the degree of

Master of Science in Electrical Engineering

University of Pittsburgh

2012

UNIVERSITY OF PITTSBURGH

SWANSON SCHOOL OF ENGINEERING

This thesis was presented

by

I-Hung Ting

It was defended on

March 29th, 2012

and approved by

Mahmoud El Nokali, PhD, Associate Professor, Department of Electrical and Computer Engineering

Joel Falk, PhD, Professor, Department of Electrical and Computer Engineering

Thesis Advisor: Hong Koo Kim, PhD, Bell of Pennsylvania/Bell Atlantic Professor, Department of Electrical and Computer Engineering

OPTICAL PROPERTIES OF SELF-ORGANIZED SILVER NANO-ISLAND THIN FILMS

I-Hung Ting, M.S.

University of Pittsburgh, 2012

For wide-spread use and large-scale implementation of photovoltaic (PV) modules, a major improvement has to be made in both energy conversion efficiency and manufacturing cost. Improving light absorption, on both spatial and spectral domains, is a critical requirement in most PV cell designs. In thin-film solar cells, in particular, light usually is not completely absorbed in single pass transmission through the active layer, therefore proper 'management' of incident photons is particularly important. Plasmonic nanostructures can play a versatile role in mediating light-matter interactions, e.g., enhancing the scattering cross-sections (metal nanoparticles), concentrating the near field intensity (metal corners and nanoapertures) and coupling of light into waveguide modes (nanogratings), potentially beneficial for enhancing light absorption.

In the study, optical properties of metal island thin films were characterized. Metal nano-islands were formed by performing thermal annealing of Ag films deposited on silica surface. The optical transmission, reflection, and extinction characteristics were analyzed for various incident angles as a function of film thickness and anneal temperature. The metal island formation is correlated to the evolution of transmission spectra, which involves surface plasmon resonance.

TABLE OF CONTENTS

LIST OF TABLES

LIST OF FIGURES

PREFACE

I appreciate Professor Hong Koo Kim for his guidance and teaching on this thesis. I also thank Siwapon Srisonphan, Myungji Kim, Dongxiao Li, Jinxuan Wu, and Zhenlv Han for their help in the lab. Finally, thanks to my family and my friends for their support and encouragement.

1.0 INTRODUCTION

Photovoltaics has been gaining renewed interest as an important source for renewable energy. Table 1.1 shows the trend and forecast of annual production of solar cells: 0.3 GW in 2000, 1.5 GW in 2005, and ultimately to 50 GW in 2020 [4].

For wide-spread use and large-scale implementation of photovoltaic (PV) modules, a major improvement has to be made in both energy conversion efficiency and manufacturing cost [1-5, 14, 15]. Improving light absorption, on both spatial and spectral domains, is a critical requirement in most PV cell designs. In thin-film solar cells, in particular, light usually is not completely absorbed in single pass transmission through the active layer, therefore proper "management" of incident photons is particularly important. Plasmonic nanostructures can play a versatile role in mediating light-matter interactions, e.g., enhancing the scattering cross-sections (metal nanoparticles), concentrating the near field intensity (metal corners and nanoapertures) and coupling of light into waveguide modes (nanogratings), potentially beneficial for enhancing light absorption [6-9, 12, 14, 18].

In the study, optical properties of metal island thin films were characterized. Metal nano-islands were formed by performing thermal annealing of Ag films deposited on silica surface. The optical transmission, reflection, and extinction characteristics were analyzed for various incident angles as a function of film thickness and anneal temperature. The metal island

formation is correlated to the evolution of transmission spectra, which involves surface plasmon resonance.

Table 1.1 Photovoltaic resource requirements: materials by production and reserve [4]

Table 1 | Photovoltaic resource requirements: materials by production and reserve.

Year	Annual solar-cell production*	Material		
		Si (c-Si)	Te (CdTe)	In ($CuInSe_2$)
2000	0.3 GW_p	4	0.03	0.03
2005	1.5 GW_p	15	0.15	0.15
2020	50 GW_p	150	5	5
World production (1,000 tonnes per year)		1,000	0.3	0.5
Reserve base (1,000 tonnes)		Abundant	47	6

*W_p = peak output power under full solar illumination.
The annual solar-cell production and the required materials feedstock are indicated, assuming cells are made of Si, CdTe or $CuInSe_2$. The assumed material use for Si is 13 g W_p^{-1} in 2000, 10 g W_p^{-1} in 2005, 3 g W_p^{-1} in 2020 (projected); it is 0.1 g W_p^{-1} for Te and In. The two bottom rows indicate the world reserve base data for Si, Te and In (that is, resources that are economic at present or marginally economic and some that are at present subeconomic).
Sources: refs 93, 94 and G. Willeke (Fraunhofer Institute for Solar Energy Systems), personal communication.

2.0 THEORY

This chapter introduces some background theories on optical reflection, transmission, refraction and surface plasmons [10-13].

2.1 FRESNEL'S FORMULAS

Plane incident wave can be split into reflected wave and transmitted wave when it is incident on the interface (Fig. 2.1) [10, 11]. The reflected wave can propagate in medium n_1, and the transmitted wave can proceed into medium n_2. If we set $E_i\exp[i(\omega t-k_i\cdot r)]$ as an incident wave, $E_r\exp[i(\omega t-k_r\cdot r)]$ and $E_t\exp[i(\omega t-k_t\cdot r)]$ should be reflected wave and transmitted wave . Here ω is frequency, and k_i, k_r and k_t are wave vectors At the interface $x = 0$, boundary conditions are

$$(k_i \cdot r)_{x=0} = (k_r \cdot r)_{x=0} = (k_t \cdot r)_{x=0}. \quad (2.1\text{-}1)$$

Since the refractive indices of media are n_1 and n_2. The magnitudes of wave vectors are

$$|k_i| = |k_r| = \frac{\omega}{c}n_1, \ |k_t| = \frac{\omega}{c}n_2. \quad (2.1\text{-}2)$$

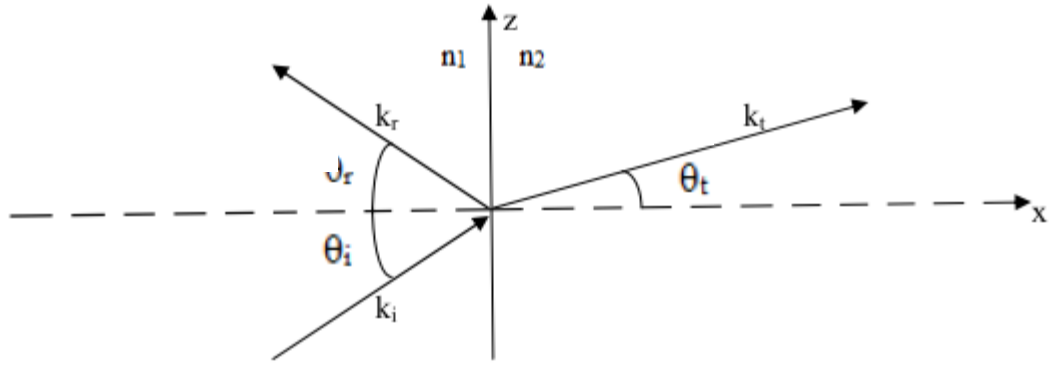

Figure 2.1 Reflection and refraction of plane wave [11]

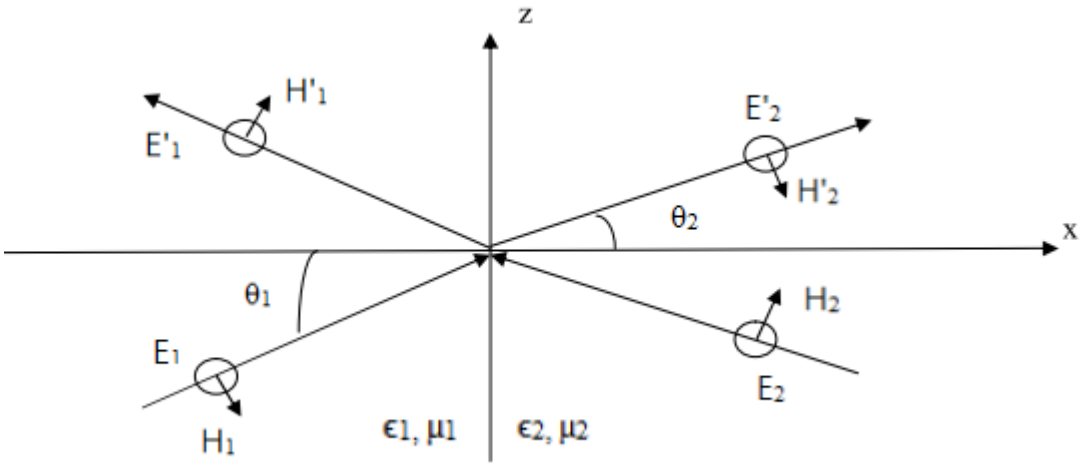

Figure 2.2 Reflection and refraction of s wave (TE) [11]

According to (2.2-1), all wave vectors must be in the same plane (Fig.2.1). The other thing is that the tangential components of wave vectors must be continuous at the interface.

Fig. 2.2 shows the case of TE polarization. The solutions of wave equation can be given in each region as follow:

$$E = \begin{cases} \left(E_1 e^{-ik_1 r} + E'_1 e^{-ik'_1 r}\right) e^{i\omega t} & x < 0 \\ \left(E_2 e^{-ik_2 r} + E'_2 e^{-ik'_2 r}\right) e^{i\omega t} & x > 0 \end{cases} . \tag{2.1-3}$$

According to Maxwell equation, the magnetic field is

$$H = \frac{i}{\omega\mu} \nabla \times E. \tag{2.1-4}$$

From Fig. 2.2, amplitude of incident wave, of reflected wave and of transmitted wave is E_1, E'_1, and E_2. Since E_1 is incident wave, E_2' should be zero. From the boundary equations,

$$\begin{cases} E_{1s} + E'_{1s} = E_{2s} + E'_{2s} \\ \sqrt{\frac{\epsilon_1}{\mu_1}} (E_{1s} - E'_{1s}) \cos\theta_1 = \sqrt{\frac{\epsilon_2}{\mu_2}} (E_{2s} - E'_{2s}) \cos\theta_2 \end{cases} \tag{2.1-5}$$

They could be rewritten as

$$D_s(1) \begin{pmatrix} E_{1s} \\ E'_{1s} \end{pmatrix} = D_s(2) \begin{pmatrix} E_{2s} \\ E'_{2s} \end{pmatrix} \tag{2.1-6}$$

Where

$$D_s(i) = \begin{pmatrix} 1 & 1 \\ \sqrt{\frac{\epsilon_i}{\mu_i}}\cos\theta_i & -\sqrt{\frac{\epsilon_i}{\mu_i}}\cos\theta_i \end{pmatrix}, \; i = 1, \; 2. \tag{2.1.7}$$

In normal case, when the incident light is from medium 1, coefficients of reflection and of transmission are

$$r_s = \left(\frac{E'_{1s}}{E_{1s}}\right)_{E_{2s}=0} , \; t_s = \left(\frac{E'_{2s}}{E_{1s}}\right)_{E_{2s}=0} . \tag{2.1-8}$$

Combining (2.1-5) and (2.1-8), we obtain

$$r_s = \frac{n_1\cos\theta_1 - n_2\cos\theta_2}{n_1\cos\theta_1 + n_2\cos\theta_2} \tag{2.1-9}$$

$$t_s = \frac{2n_1\cos\theta_1}{n_1\cos\theta_1 + n_2\cos\theta_2} . \tag{2.1-10}$$

On the other hand, if we evaluate the p wave (TM Wave) with the same method, we can get

$$r_p = \frac{n_1\cos\theta_2 - n_2\cos\theta_1}{n_1\cos\theta_2 + n_2\cos\theta_1} \tag{2.1-11}$$

$$t_p = \frac{2n_1\cos\theta_1}{n_1\cos\theta_2 + n_2\cos\theta_1} . \tag{2.1-12}$$

Reflectance and transmittance are:

$$R_s = |r_s|^2 \tag{2.1-13}$$

$$R_p = |r_p|^2 \tag{2.1-14}$$

$$T_s = \frac{n_2 \cos\theta_2 |t_s|^2}{n_1 \cos\theta_1} \tag{2.1-15}$$

$$T_p = \frac{n_2 \cos\theta_2 |t_p|^2}{n_1 \cos\theta_1} \ . \tag{2.1-16}$$

2.2 BREWSTER ANGLE

Referring to Fig. 2.2, r_s and r_p vary depending on the incident angle. R_p is always smaller than R_s. Moreover, the condition for R_p to vanish is that

$$n_2 \cos\theta_1 = n_1 \cos\theta_2. \tag{2.2-1}$$

If we use the Snell's law, we could obtain the following expression for this particular angle

$$\theta_B = \tan^{-1} \frac{n_2}{n_1}. \tag{2.2-2}$$

This angle is called Brewster's angle [11]. From (2.2-1) and (2.2-2), r_p would be zero when $\theta_1 + \theta_2 = \frac{1}{2}\pi$. In other words, when the reflected wave and the transmitted wave are orthogonal, the reflectance for TM wave would vanish.

2.3 SURFACE PLASMON

Surface plasmons are coherent fluctuations of electron density at metal/dielectric interface, carrying electromagnetic energy as a surface bound wave [10, 12, 13].

Assume an interface of semi-infinite medium (ε_1) and air (ε_2). If TM wave propagates on the interface along x direction, the fields are:

$$Z > 0 \qquad \begin{matrix} H_2 = (0, H_{y2}, 0)\exp i(k_{x2}x + k_{z2}z - \omega t) \\ E_2 = (E_{x2}, 0, E_{z2})\exp i(k_{x2}x + k_{z2}z - \omega t) \end{matrix} \tag{2.3-1}$$

$$Z < 0 \qquad \begin{matrix} H_1 = (0, H_{y1}, 0)\exp i(k_{x1}x - k_{z1}z - \omega t) \\ E_2 = (E_{x1}, 0, E_{z1})\exp i(k_{x1}x - k_{z1}z - \omega t) \end{matrix} \tag{2.3-2}$$

where magnetic field H and electric field E should satisfy Maxwell's equation (2.1-4).

These fields should also satisfy the continuity conditions:

$$E_{x1} = E_{x2} \tag{2.3-3}$$

$$H_{y1} = H_{y2} \tag{2.3-4}$$

$$\varepsilon_1 E_{z1} = \varepsilon_2 E_{z2} \tag{2.3-5}$$

$$k_{x1} = k_{x2} = k_x \, . \tag{2.3-6}$$

They can fulfill Maxwell's equation as well

$$\frac{\partial H_{yi}}{\partial z} = -\varepsilon_i E_{xi} \frac{\omega}{c} \, . \tag{2.3-7}$$

Combing (2.3-3), (2.3-4), and (2.3-7), we could get

$$\frac{k_{z1}}{\varepsilon_1} H_{y1} + \frac{k_{z2}}{\varepsilon_2} H_{y2} = 0. \tag{2.3-8}$$

To modify above equations,

$$\frac{k_{z1}}{\varepsilon_1} + \frac{k_{z2}}{\varepsilon_2} = 0 \tag{2.3-9}$$

$$k_x = \frac{\omega}{c}\left(\frac{\varepsilon_1 \varepsilon_2}{\varepsilon_1 + \varepsilon_2}\right)^{\frac{1}{2}} . \tag{2.3-10}$$

Thus, when medium $\varepsilon_1 < 0$ and medium $\varepsilon_2 = 1$, the maxima of fields is at z = 0. Then, the incident wave can be presented

$$E = E_0^{\pm} \exp[+i(k_x x \pm k_z z - \omega t)] \tag{2.3-11}$$

which can cause the decay of E_z. The wave vector k_x should be parallel to x direction, $k_x = \frac{2\pi}{\lambda_p}$ where λ_p is the resonance wavelength. k_x could also fulfill (2.3-10).

In the normal case, medium 2 is air. Therefore, SP propagation constant becomes

$$k_x = k_{sp} = \frac{\omega}{c}\sqrt{\frac{\varepsilon_m \varepsilon_a}{\varepsilon_m + \varepsilon_a}} = \frac{\omega}{c}\sqrt{\frac{(\varepsilon_{mr} + i\varepsilon_{mi})\varepsilon_d}{(\varepsilon_{mr} + i\varepsilon_{mi}) + \varepsilon_d}}. \tag{2.3-12}$$

According to (2.3-12), SP effective index should be

$$n_{eff}=\frac{k_{sp}}{k_0} \tag{2.3-13}$$

and propagation length is

$$L_{sp}=\frac{1}{2\mathrm{Im}(k_x)} \ . \tag{2.3-14}$$

Assuming $\left|\frac{\varepsilon_m}{\varepsilon_{mr}}\right| \ll 1$ and $\left|\frac{\varepsilon_{mi}}{\varepsilon_{mr}+\varepsilon_a}\right| \ll 1$, the propagation constant should be

$$k_{sp}=\frac{\omega}{c}\left(\frac{\varepsilon_m\varepsilon_a}{\varepsilon_m+\varepsilon_a}\right)^{\frac{1}{2}}+i\frac{\omega}{c}\left(\frac{\varepsilon_m\varepsilon_a}{\varepsilon_m+\varepsilon_a}\right)^{\frac{3}{2}}\frac{\varepsilon_{mi}}{2(\varepsilon_{mr})^2} \tag{2.3-15}$$

and the resonance frequency is

$$\omega_1=\frac{\omega_p}{\sqrt{1+\varepsilon_0}}=\frac{\omega_p}{\sqrt{2}} \ . \tag{2.3-16}$$

Therefore, when light incident from air to metal, we can not only evaluate Fresnel's formulas, but also assess surface plasmon phenomena.

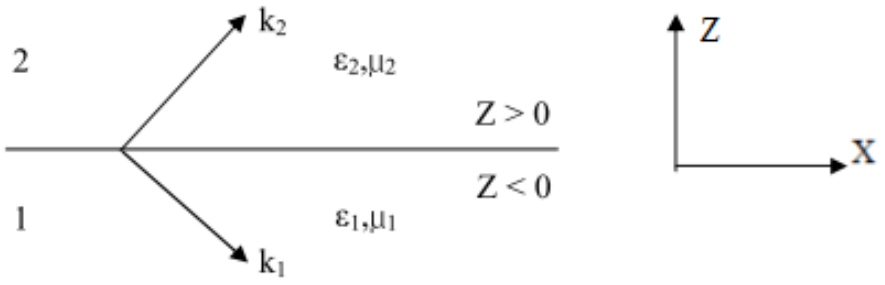

Figure 2.3 Scheme of the interface between two media on which the SP propagates [12]

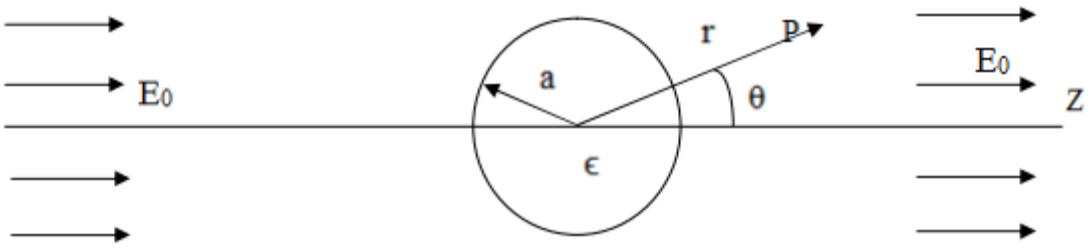

Figure 2.4 Electric field interact with metal particle

However, we should consider particle surface plasmon as well [12, 13, 17]. Assuming the light interact with particle, we can get these two equations

$$\nabla^2\Phi = 0 \tag{2.3-17}$$

$$\frac{1}{r^2}\frac{\partial}{\partial r}\left(r^2\frac{\partial\Phi}{\partial r}\right)+\frac{1}{r^2\sin\theta}\frac{\partial}{\partial\theta}\left(\sin\theta\frac{\partial\Phi}{\partial\theta}\right)+\frac{1}{r^2\sin^2\theta}\frac{\partial^2\Phi}{\partial\phi^2}=0 \tag{2.3-18}$$

where Φ is potential (Figure 2.4).

To modify (2.3-18), we can get the solution

$$\Phi=\sum_{n=0}^{\infty}\sum_{m=0}^{\infty}\left(a_{nm}r^n+\frac{b_{nm}}{r^{n+1}}\right)P_n^m(\cos\theta)e^{im\phi} \quad . \tag{2.3-19}$$

When r < a (inside the sphere), the solution is

$$\Phi_{in} = \sum_{l=0}^{\infty}A_l r^l P_l(\cos\theta) \ ; \tag{2.3-20}$$

when r > a (outside the sphere), the solution is

$$\Phi_{out} = \sum_{l=0}^{\infty}\left(B_l r^l + C_l r^{-(l+1)}\right)P_l(\cos\theta). \tag{2.3-21}$$

The following equations are boundary conditions:

$$r = \infty \qquad \Phi_{out} = -E_0 z = -E_0 r\cos\theta \tag{2.3-22}$$

$$r = a \qquad -\frac{1}{a}\frac{\partial \Phi_{in}}{\partial \theta}\Big|_{r=a} = -\frac{1}{a}\frac{\partial \Phi_{out}}{\partial \theta}\Big|_{r=a} \tag{2.3-23}$$

$$r = a \qquad -\varepsilon\frac{\partial \Phi_{in}}{\partial \theta}\Big|_{r=a} = -\varepsilon_0\frac{\partial \Phi_{out}}{\partial \theta}\Big|_{r=a}. \tag{2.3-24}$$

Combing (2.3-20), (2.3-21), (2.3-22), (2.3-23), and (2.3-24), answers can be presented as:

$$\Phi_{in} = -\left(\frac{3}{\frac{\varepsilon}{\varepsilon_0}+2}\right)E_0 r\cos\theta \tag{2.3-25}$$

$$\Phi_{out} = -E_0 r\cos\theta + \left(\frac{\frac{\varepsilon}{\varepsilon_0}-1}{\frac{\varepsilon}{\varepsilon_0}+2}\right)E_0\frac{a^3}{r^2}\cos\theta \tag{2.3-26}$$

According to Maxwell's equation, electric fields can be written as:

$$E_{in} = \left(\frac{3}{\frac{\varepsilon}{\varepsilon_0}+2}\right)\left(E_0\cos\theta e_r - E_0\sin\theta e_\theta\right) = \left(\frac{3}{\frac{\varepsilon}{\varepsilon_0}+2}\right)E_0 e_z \tag{2.3-27}$$

$$E_{out} = E_o e_z + \left(\frac{\frac{\varepsilon}{\varepsilon_0}-1}{\frac{\varepsilon}{\varepsilon_0}+2}\right)\frac{a^3}{r^3}E_0(2\cos\theta e_r + \sin\theta e_\theta) \tag{2.3-28}$$

$$p = 4\pi\varepsilon_0\left(\frac{\frac{\varepsilon}{\varepsilon_0}-1}{\frac{\varepsilon}{\varepsilon_0}+2}\right)a^3 E_0 \tag{2.3-29}$$

$$P = \frac{p}{V} = \frac{p}{\frac{4}{3}\pi a^3} = 3\varepsilon_0\left(\frac{\frac{\varepsilon}{\varepsilon_0}-1}{\frac{\varepsilon}{\varepsilon_0}+2}\right)E_0 \tag{2.3-30}$$

Therefore, the condition of particle surface plasmon resonance is

$$\varepsilon = -2\varepsilon_0 \tag{2.3-31}$$

and resonance frequency is

$$\omega_2 = \frac{\omega_p}{\sqrt{1+2\varepsilon_0}} = \frac{\omega_p}{\sqrt{3}} \quad . \tag{2.3-32}$$

2.4 SCATTERING CROSS SECTION

Metal islands can behave like microscopic antennas, which can collect the radiation and transfer energy into waveguide. On the other hand, it can influence scattering and absorbing significantly when the wavelength is near resonance wavelength since the cross-sectional area could be larger than geometric cross-sectional area [1, 4-8, 16].

For small particles, the scattering and absorption cross sections are given by

$$C_{abs} = \frac{2\pi}{\lambda} \mathrm{Im}[\alpha] \tag{2.4-1}$$

and

$$C_{sca} = \frac{1}{6\pi} \left(\frac{2\pi}{\lambda}\right)^4 |\alpha|^2. \tag{2.4-2}$$

Here, α is the polarizability, which is

$$\alpha=3V\frac{\varepsilon-1}{\varepsilon+2} \tag{2.4-3}$$

where V is the particle's volume and ε is the permittivity of metal. The scattering efficiency is

$$Q_{sca}=\frac{C_{sca}}{C_{sca}+C_{abs}} \ . \tag{2.4-4}$$

Then, the polarizability α could be divided by two parts: $\alpha_R(\omega)$ is along the major axes; $\alpha_z(\omega)$ is along minor axes. Assume ε_{11} is the real part of $\alpha_R(\omega)$ and ε_{10} is the real part of $\alpha_z(\omega)$, they could be described

$$\alpha_R(\omega)=\frac{V}{2\pi Q}\frac{\varepsilon(\omega)-1}{\varepsilon(\omega)-\varepsilon_{11}} \tag{2.4-5}$$

and

$$\alpha_z(\omega)=\frac{V}{4\pi(1-Q)}\frac{\varepsilon(\omega)-1}{\varepsilon(\omega)-\varepsilon_{10}} \ . \tag{2.4-6}$$

Finally, we could get that the total cross section

$$\sigma=\frac{4\pi\omega}{c}\mathrm{Im}(\alpha_R\cos^2\theta+\alpha_z\sin^2\theta). \tag{2.4-11}$$

If metal particles are smaller than the wavelength of light, the absorption and the extinction can be enhanced. Besides the metal particle's size, their shape, material, and refractive index of the surrounding medium can influence the phenomena [1, 4-8, 16]. Therefore, when we modify these conditions, the phenomena of surface plasmons, reflection, transmission, and refraction can be affected.

3.0 METHOD

This chapter describes experimental procedures: cleaning, thermal evaporation, annealing, and optical characterization.

3.1 CLEANING

Sample fabrication involves multiple steps of preparation. First a silica wafer was covered with wax. Then, diamond saw was used to cut the wafer into square pieces (Fig 3.1). After cutting, the silica samples were cleaned by chemical solutions in the following steps.

First, rinsed in acetone for five minutes, and the remaining wax was removed by cotton swabs. Then, the sample was placed into acetone and was sonicated for 5 minutes. The cleaning step was repeated with methanol, and then finally the sample was rinsed in D.I. water.

The wafers were blown dried by nitrogen gas. Finally, the samples were placed in the oven and dried for 30 minutes at $90^{o}C$~$100^{o}C$ to remove moisture.

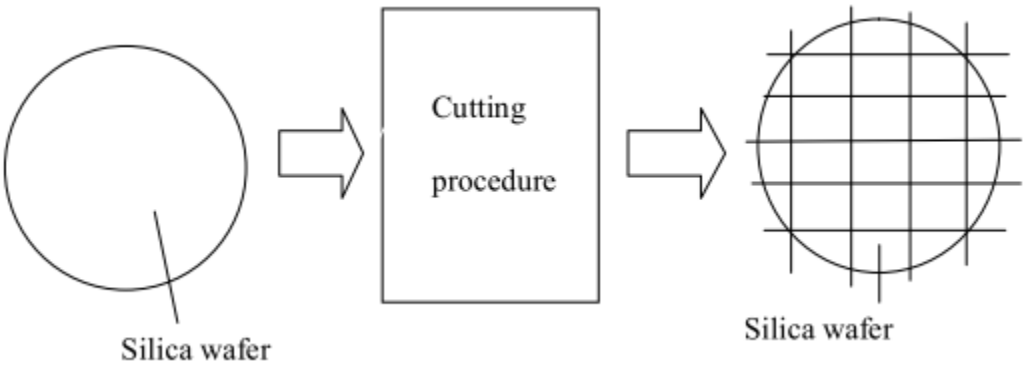

Figure 3.1 Cutting samples

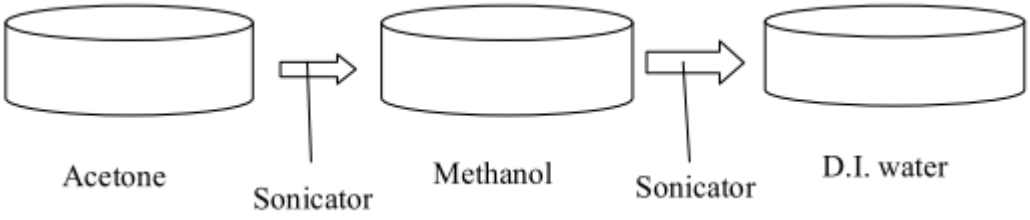

Figure 3.2 Cleaning procedure

3.2 THERMAL EVAPORATION

After cleaning the silica samples, silver was deposited by thermal evaporation. The silica samples were placed on microscope glass slide, and it was partly covered by thin cover glass (Fig. 3.3). The step made by this cover glass is for film thickness measurement.

Thermal evaporation was performed at base pressure better than $8x10^{-5}$ mTorr. The deposition rate was ~0.1 nm/s.

3.3 ANNEALING

Annealing was the next step. At first, the annealing chamber should be dry and the power was also turned on. Samples were introduced to the chamber when the temperature was higher than the condition of experiment because the temperature might decrease when we opened the annealing chamber. For example, if the temperature of our purpose was 250^{o}C, we should heat up to 260^{o}C then mount the samples. Gas flow was monitored to control the flow rate and stabilize the annealing condition. Then, the samples were put in the annealing chamber which is connected with forming gas (90% nitrogen and 10% hydrogen).

One important thing was that the step with forming gas should be operated in the fume hood since hydrogen is explosive. The annealing time is 30 minutes. During the 30-minute interval, the forming gas flown into the annealing chamber continuously and the temperature maintained stable. According to silver's properties, oxidation should be avoided. Therefore, we turned off the power but not forming gas after annealing. When the temperature was reduced to 70^{o}C in the annealing chamber, the forming gas could be turned off and samples were retrieved.

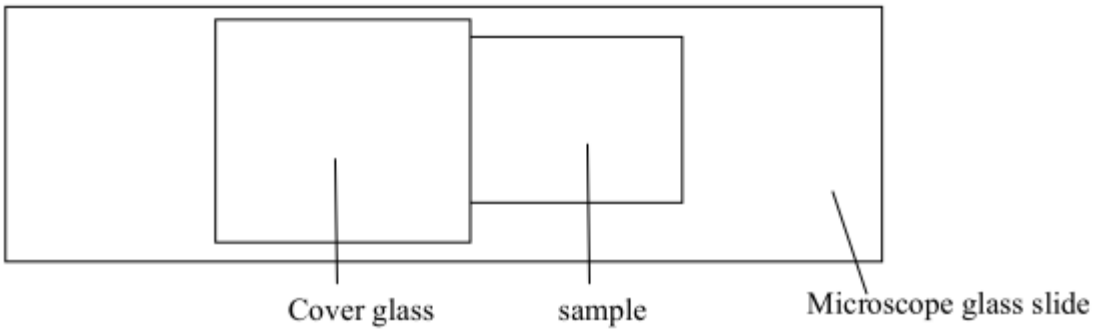

Figure 3.3 Samples on microscope glass slide

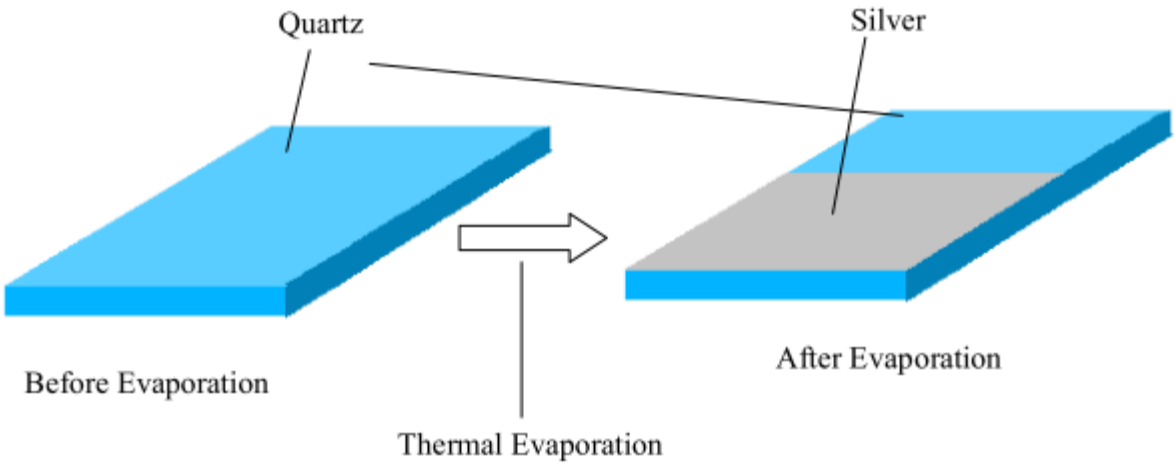

Figure 3.4 Difference between samples

3.4 MEASUREMENT

The optical properties of metal islands on thin films were characterized by measuring the thin film reflectance and transmittance. The angular dependence of reflectance and transmittance at wavelength of 633 nm were measured by using a goniometric step with He-Ne laser. The normal-incidence transmission spectra were measured by a CCD spectrometer.

Fig. 3.5 shows the schematic of the goniometric setup for the angular dependence of reflection and transmission measurements. The laser is linearly polarized, and the TE mode or TM mode (relative to the sample) can be adjusted by rotating the laser tube. After metal deposition and annealing, the sample was mounted on the holder. The power of the incident, reflected and transmitted laser beam at different angle were measured by a power detector (LM-2). After normalization, we can get angular dependence of reflectance and transmittance. The powers of laser beam were measured every five degree from -80 degree to 80 degree. To minimize experimental errors in changing the angles, the measurement at the angles with the same absolute values were conducted at the same time. For example: the reflection and transmission at 5 degree was measured and then measurement at -5 degree was followed. The measuring procedure was: 0^o, 5^o, -5^o, 10^o, -10^o, 15^o, -15^o, and so on.

The transmission spectra were measured by a CCD spectrometer. In the procedure, the light source was the combo of Deuterium and Tungsten sources (Edmund BDS100, S/N: 040512302). The light was incident normally to the sample, collected by a fiber patch cord, and detected by the CCD spectrometer (Edmund No-BRC111A-USB-VIS/NIR, S/N: 070123362). The CCD spectrometer was connected to a computer to obtain the spectra data. The dark spectrum and the

reference spectrum were measured. The reference sample was a quartz substrate without metal. The transmittance was calculated by the equation:

$$\text{Transmittance} = \frac{\text{Raw data} - \text{Dark spectrum}}{\text{Reference spectrum} - \text{Dark spectrum}}. \quad (3.4\text{-}1)$$

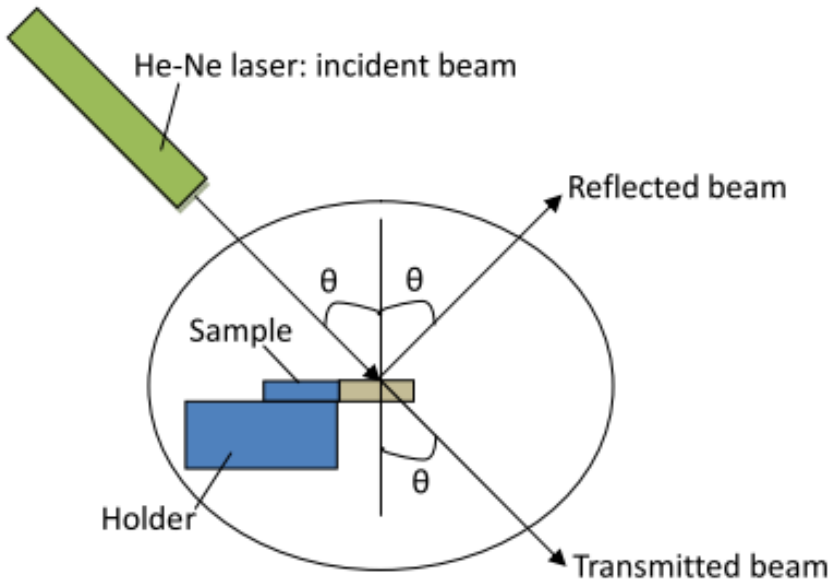

Figure 3.5 Setup for reflection and transmission measurements

4.0 RESULT AND ANALYSIS

This chapter describes the results of reflection, transmission, and extinction measurements.

4.1 ANALYSIS–REFLECTANCE AT 633 NM WAVELENGTH

Figure 3.5 shows that reflectance is

$$\text{Reflectance} = \frac{I_R}{I_{inc}} \tag{4.2-1}$$

where I_{inc} is power of incident beam and I_R is power of reflection beam. If the incident beam is TM wave, Brewster's angles can be calculated by equation (2.2-2). 57 degree and -57 degree are Brewster's angles of silica.

4.1.1 Reflectance of samples with the same thickness at different annealing temperatures

From Fig. 4.1 to Fig. 4.4, the thickness of silver is fixed and the annealing temperature was varied. The dashed lines represent the theoretical calculation of silica. Brewster's angles appear for TM mode.

When the thickness of silver is 30 nm, the reflectances of the samples are always very high as shown in Fig. 4.1.

In Fig. 4.2, when the thickness of silver is 20 nm, the reflectances of the annealed samples are lower than that of the un-annealed samples since big metal islands can be formed. There are two valleys which are close to Brewster's angles for TM mode after annealing. In other words, big metal islands can be formed, so the distributions of silica of the annealed samples which can interact with light are more than that of the un-annealed samples.

When the thickness of silver is 15 nm and 20 nm, the phenomenon is much clear as shown in Fig. 4.3 and Fig. 4.4. Thus, the most vital phenomenon is that the reflectances of the annealed samples are lower than that of the un-annealed samples when the thickness of silver is thinner than 20 nm. In other words, after annealing, big metal islands can be formed when the thickness of silver is less than 20 nm.

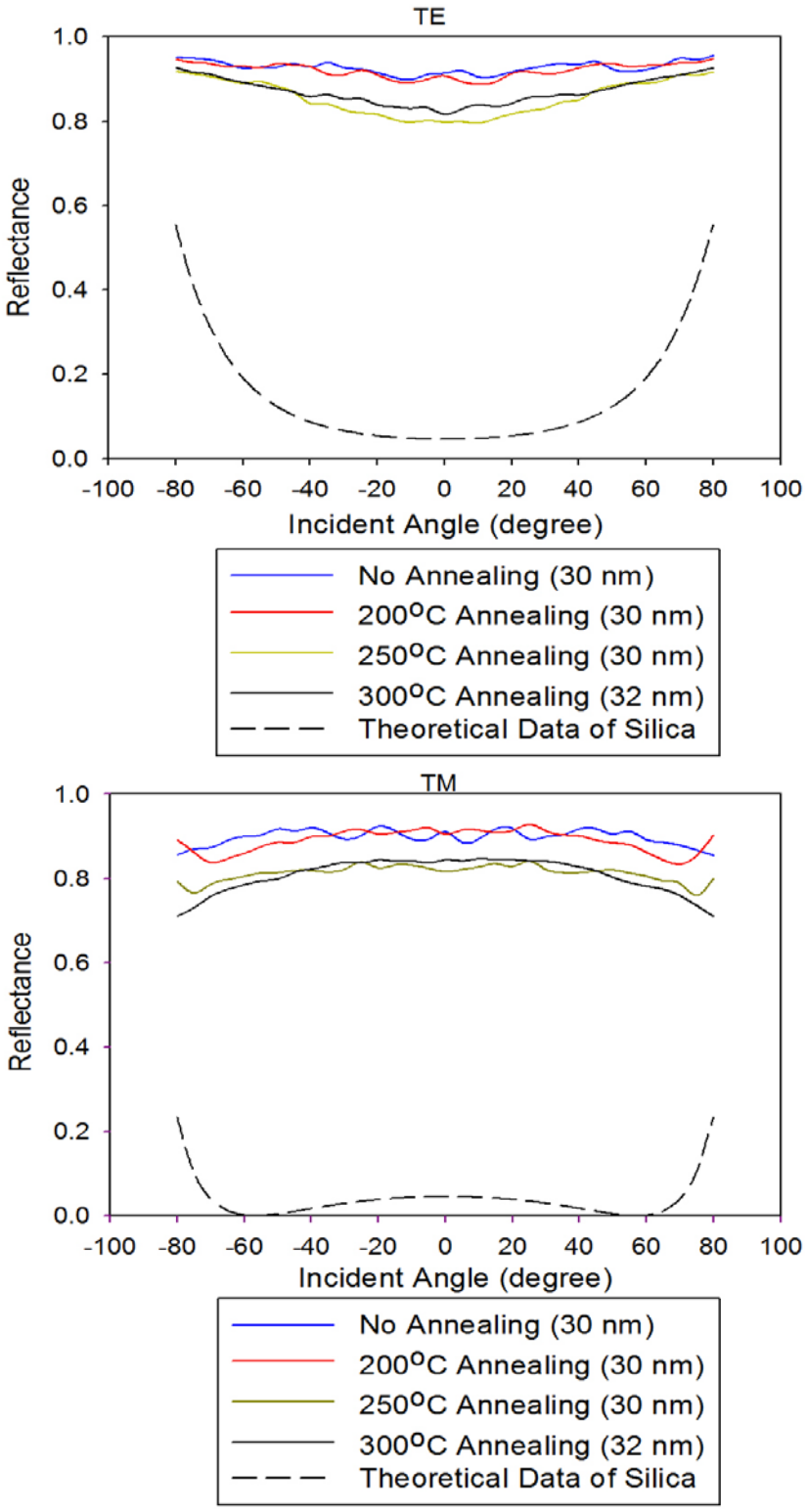

Figure 4.1 Reflectance of silver islands with 30 nm thickness at different annealing temperatures

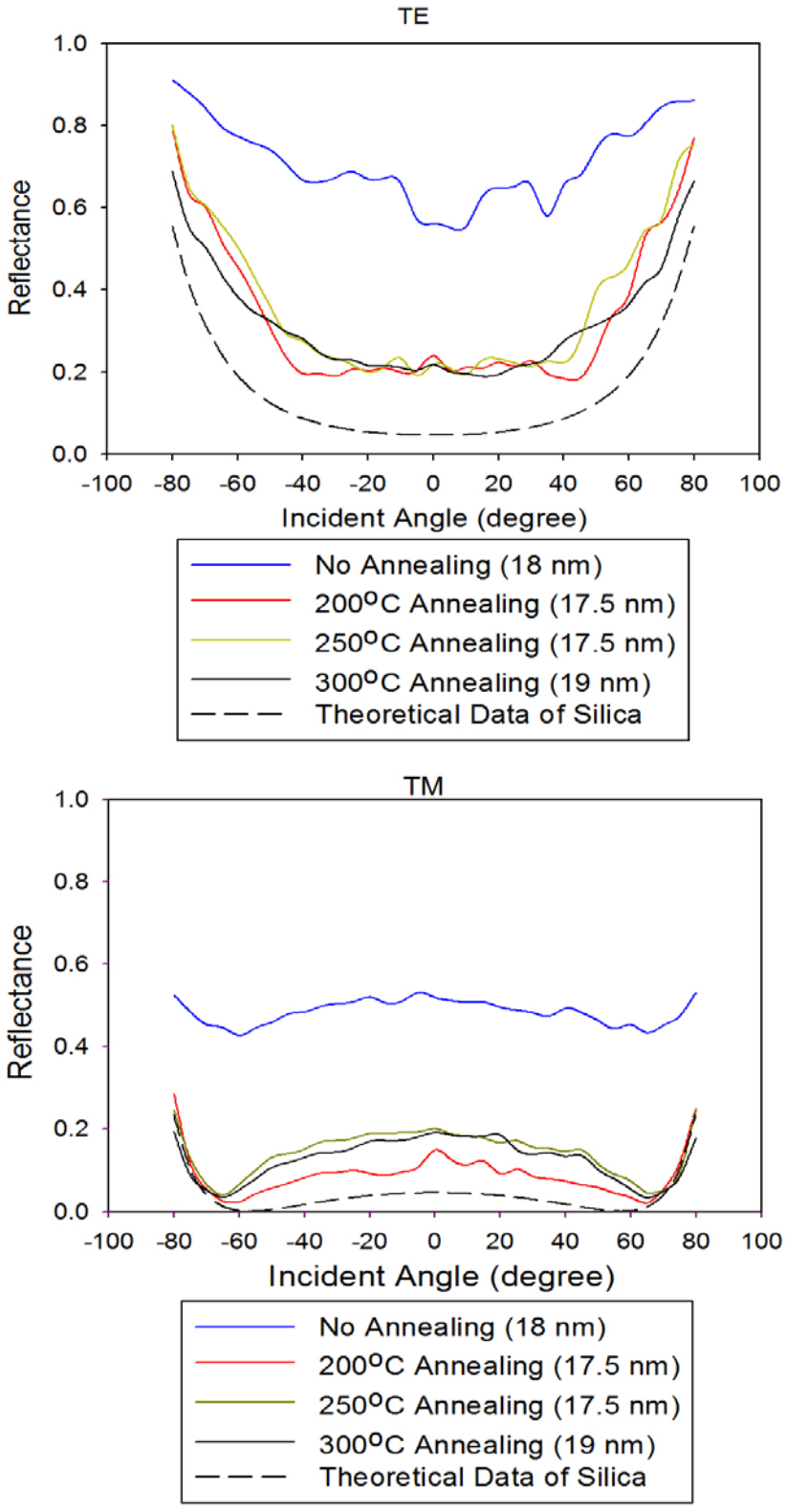

Figure 4.2 Reflectance of silver islands with 20 nm thickness at different annealing temperatures

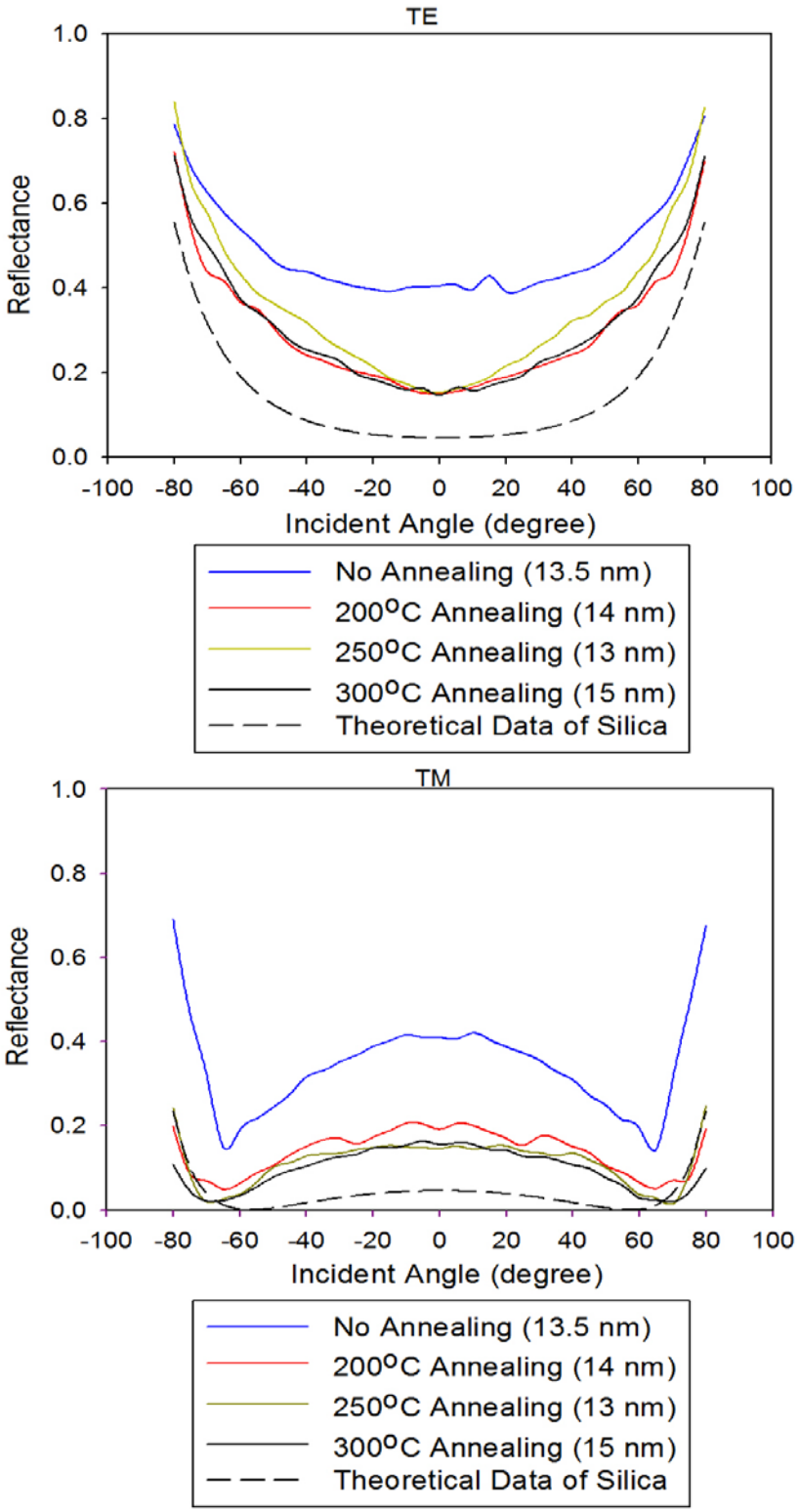

Figure 4.3 Reflectance of silver islands with 15 nm thickness at different annealing temperatures

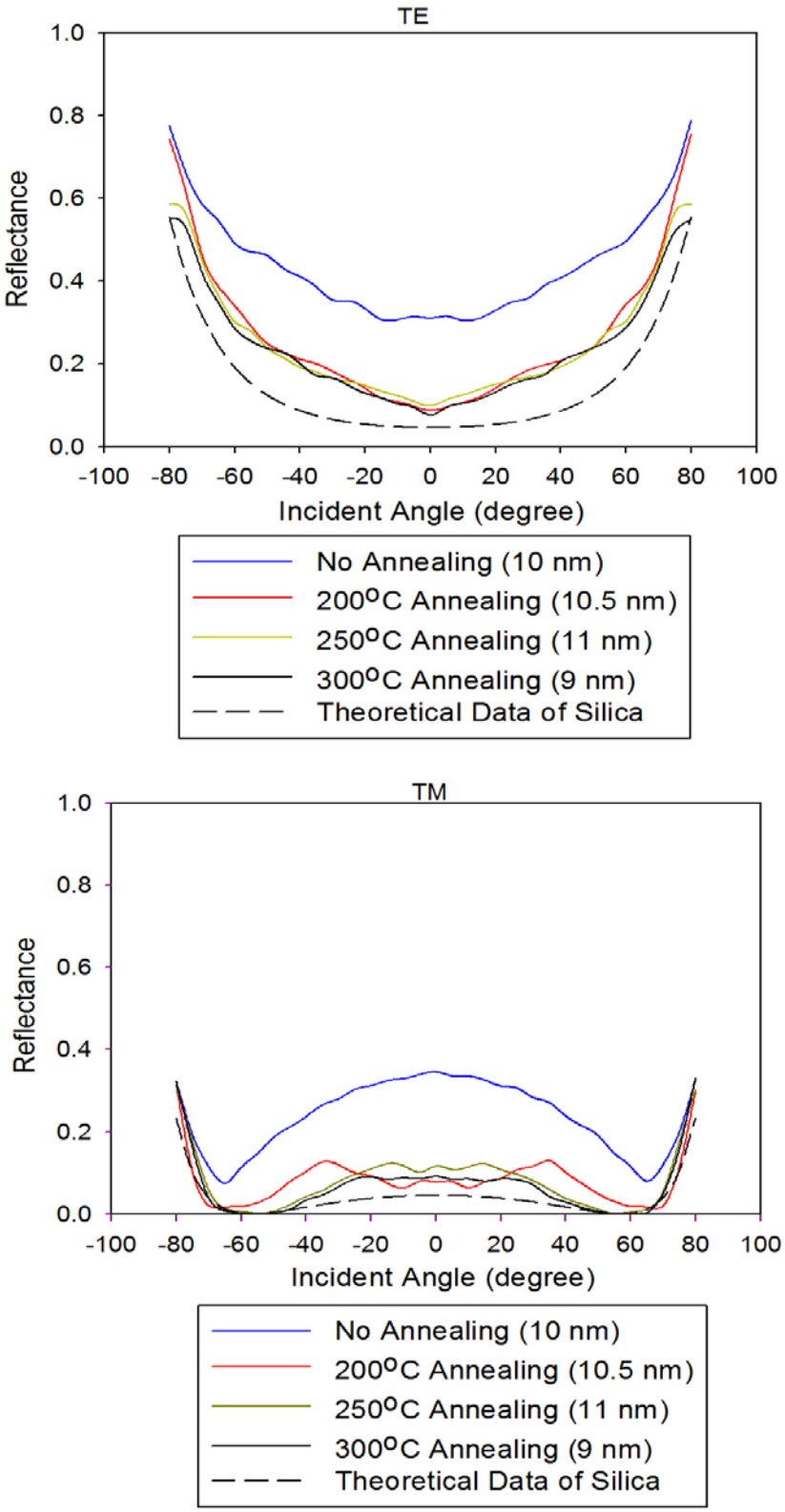

Figure 4.4 Reflectance of silver islands with 10 nm thickness at different annealing temperatures

4.1.2 Reflectance of samples with different thicknesses at the same annealing temperature

From Fig. 4.5 to Fig. 4.8, it's clear that annealing can dramatically influence the reflectance. The reflectances of samples with 30 nm silver thickness are higher than that of samples with 20 nm silver thickness, 15 nm silver thickness and 10 nm silver thickness as shown in Fig. 4.5. However, in Fig. 4.5, there are Brewster's angles for TM mode when the thickness of silver is 15 nm and 10 nm. In other words, light might interact with silica directly before annealing since the thickness is thin.

In Fig. 4.6, the reflectances of samples with 30 nm silver thickness is much higher than that of samples with others. When the thickness of silver is less than 20 nm, big metal islands can be formed since the reflectances are close to dash lines and there are Brewster's angles for TM mode.

If the annealing temperature increases to 250^{o}C and 300^{o}C, the phenomenon of reflectance is similar to that observed at 200^{o}C as shown in Fig. 4.7 and Fig. 4.8. The only difference is that the reflectances of samples with 20 nm silver thickness are higher than that of samples with 15 nm silver thickness as shown in Fig. 4.7 and Fig. 4.8. The reflectances of samples with 15 nm silver thickness should be stable when the annealing temperature is higher than 200^{o}C since the thickness is thin and big metal islands can be formed easily. However, the reflectances of samples with 20 nm silver thickness should be stable when the annealing temperature is higher than 250^{o}C. Thus, the reflectances of samples with 20 nm silver thickness are lower than that of samples with 15 nm silver thickness when the annealing temperature is 200^{o}C, but the phenomenon is reversed when the annealing temperature is higher than 250^{o}C. We'll get more information in the following discussion.

In sum, big metal islands can be formed when the thickness of silver is less than 20 nm and the annealing temperature is higher than 200^{o}C. However, when the annealing temperature is higher than 250^{o}C, the effects might be stable with 20 nm and 15 nm.

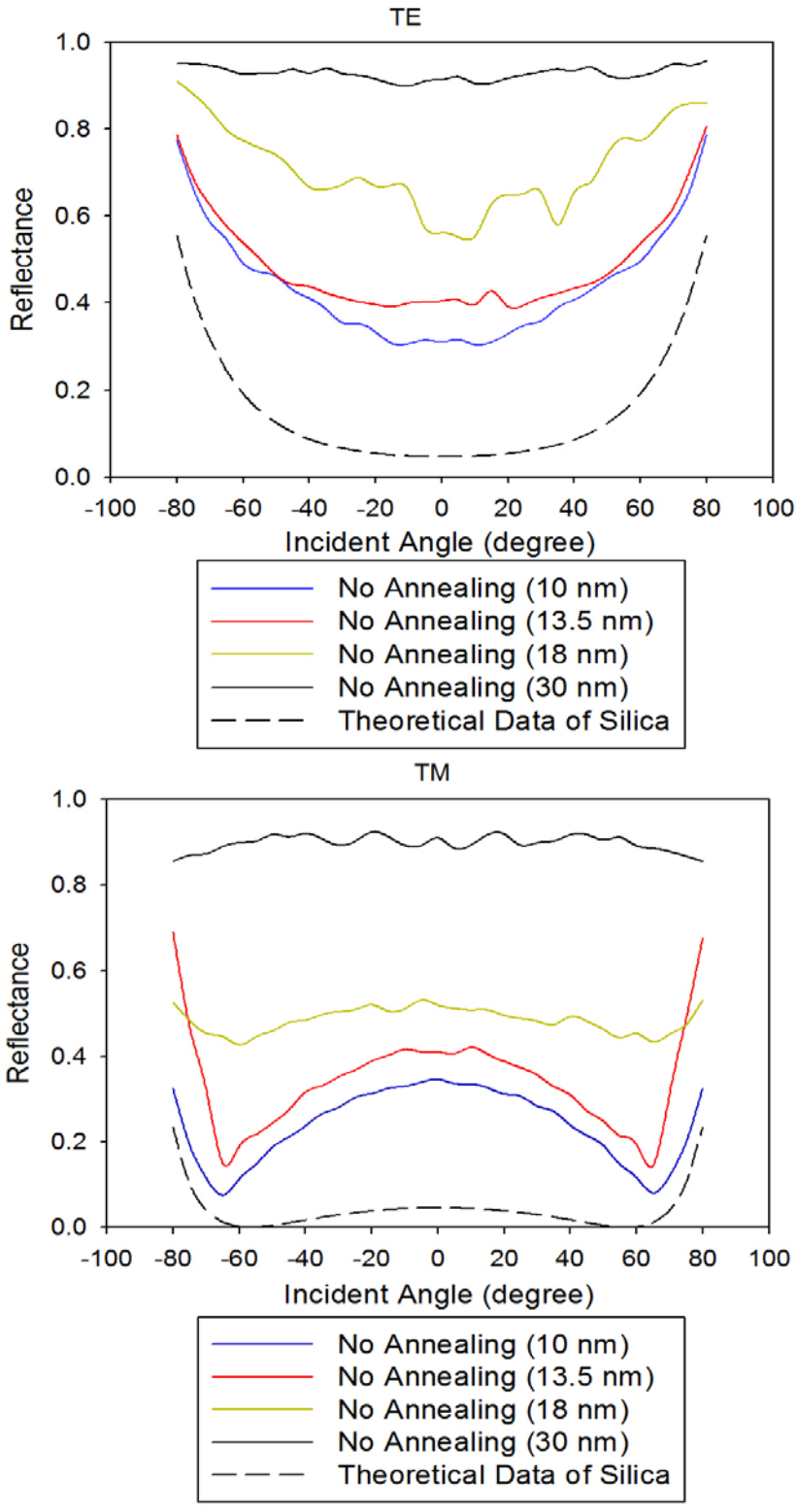

Figure 4.5 Reflectance of silver islands with different thicknesses

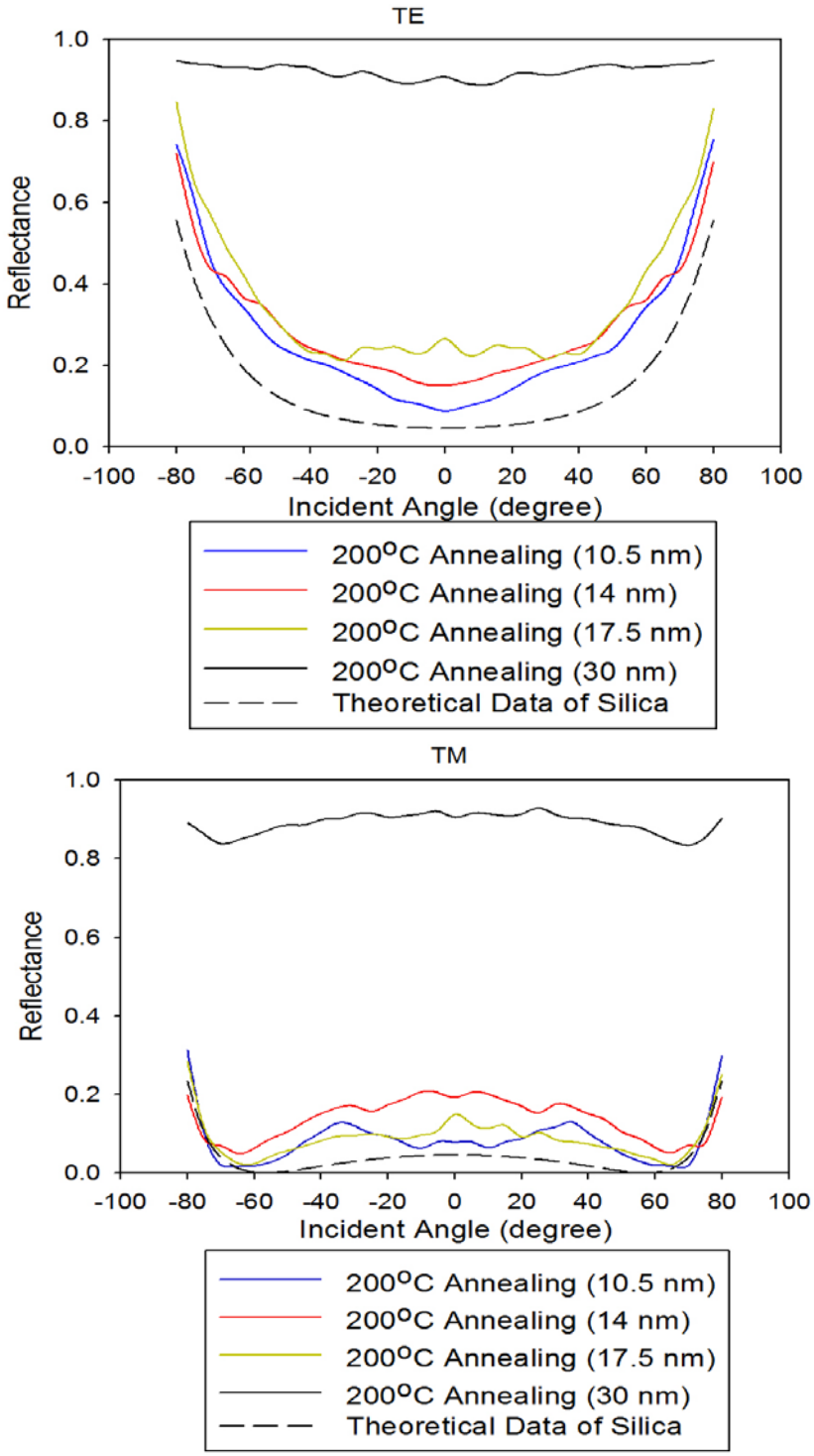

Figure 4.6 Reflectance of silver islands with different thicknesses at 200°C annealing temperature

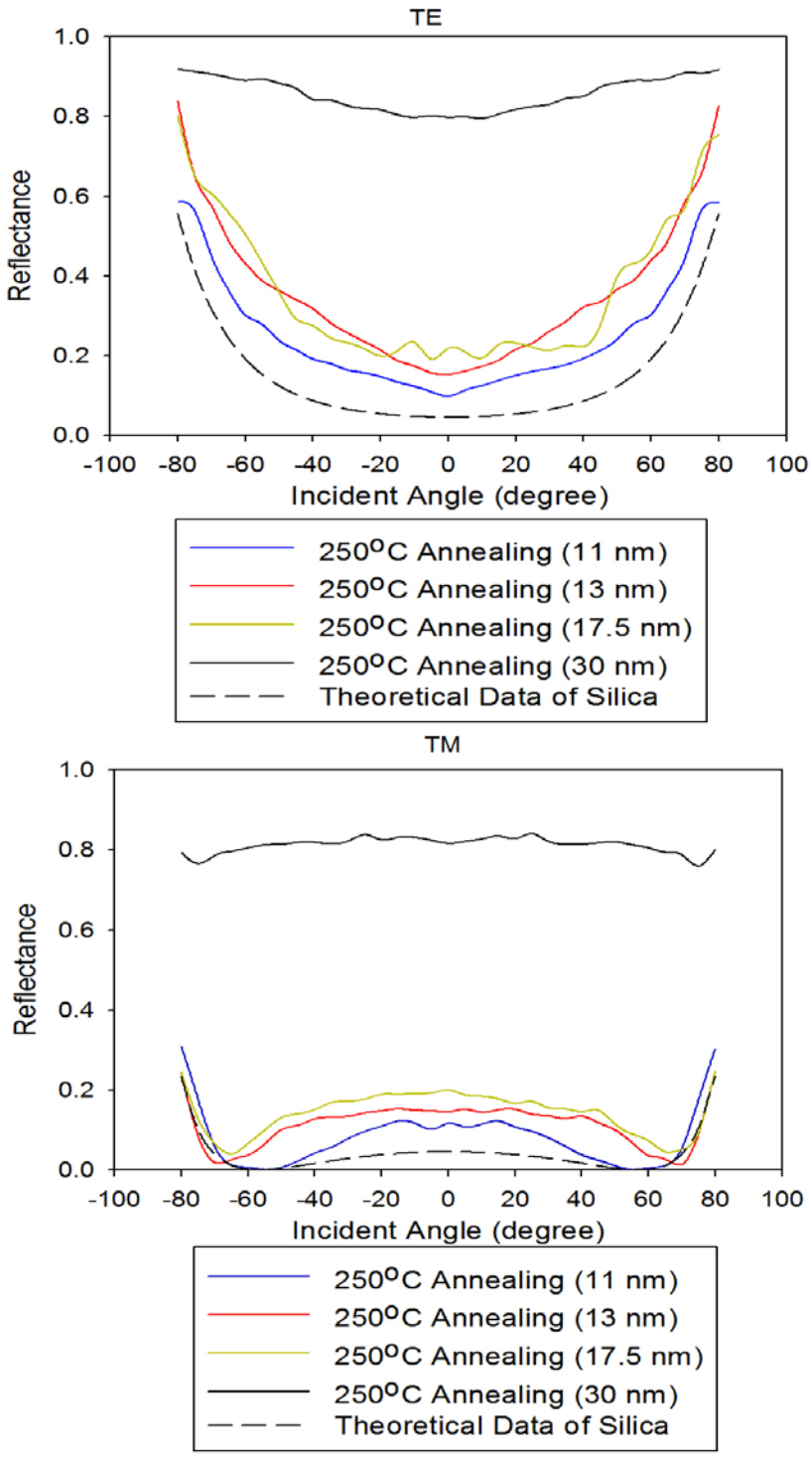

Figure 4.7 Reflectance of silver islands with different thicknesses at 250°C annealing temperature

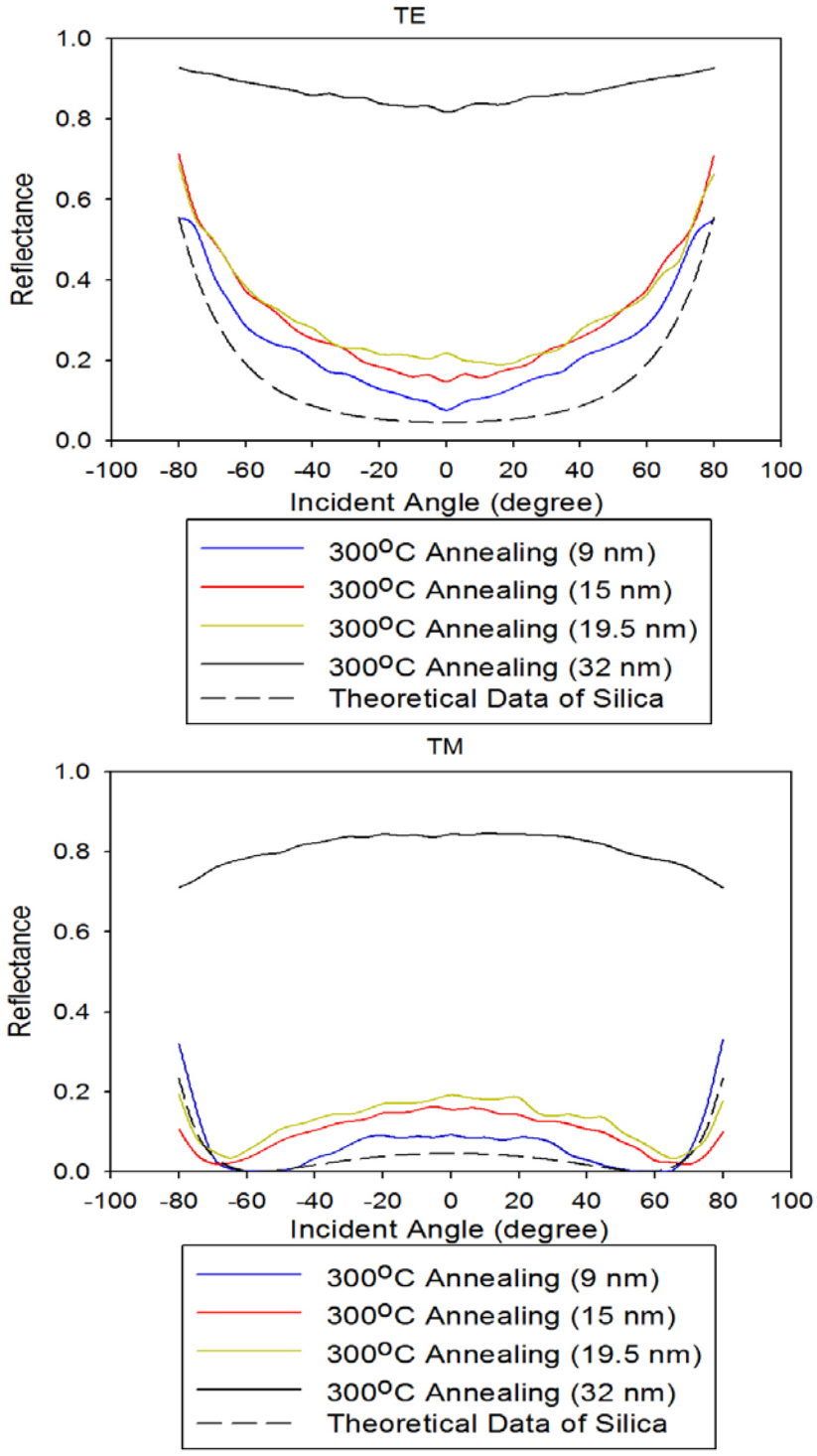

Figure 4.8 Reflectance of silver islands with different thicknesses at 300°C annealing temperature

4.2 ANALYSIS–TRANSMITTANCE AT 633 NM WAVELENGTH

According to Fig. 3.5, the transmittance is

$$\text{transmittance} = \frac{I_T}{I_{inc}} \tag{4.3-1}$$

where I_{inc} is power of incident beam and I_T is power of transmission beam.

4.2.1 Transmittance of samples with the same thickness at different annealing temperatures

In Fig. 4.9, the transmittances are very low because the thickness of silver is very thick and the properties of samples are like silver.

In Fig. 4.10, for TE mode, the transmittance of the un-annealed sample is lower than that of the annealed samples but the difference is not large. In other words, big metal islands can be formed after annealing but the effects are not obvious. For TM mode, the transmittance of the un-annealed sample is similar to that of the annealed samples. According to the discussion in the reflectance and the transmittance of samples with 20 nm silver thickness for TE mode, big metal islands should be formed after annealing. It means that silver islands of the top layer might form big metal islands but silver islands of the bottom layer might still be continuous.

However, when the thickness of silver is 15 nm, the phenomena are different. In Fig. 4.11, the transmittances of the un-annealed samples are lower than that of the annealed samples, and the transmittances of each annealed samples are similar. On the other hand, big metal islands are formed and the effects are clear after annealing.

In Fig. 4.12, when the annealing temperature is higher than 250^{o}C, the transmittances of samples at 250^{o}C are similar to that of samples at 300^{o}C albeit both transmittances are higher than that of samples at 200^{o}C. The thinner the thickness is, the fewer the number of silver islands. When the thickness of silver is 10 nm, the number of silver islands is quite few. After annealing, big metal islands can be formed easily. When the annealing temperature is 250^{o}C, all silver islands can form big metal islands. Even though the annealing temperature is higher than 250^{o}C, the number of metal islands is the same. Thus, the transmittances of samples at 250^{o}C are similar to that of samples at 300^{o}C.

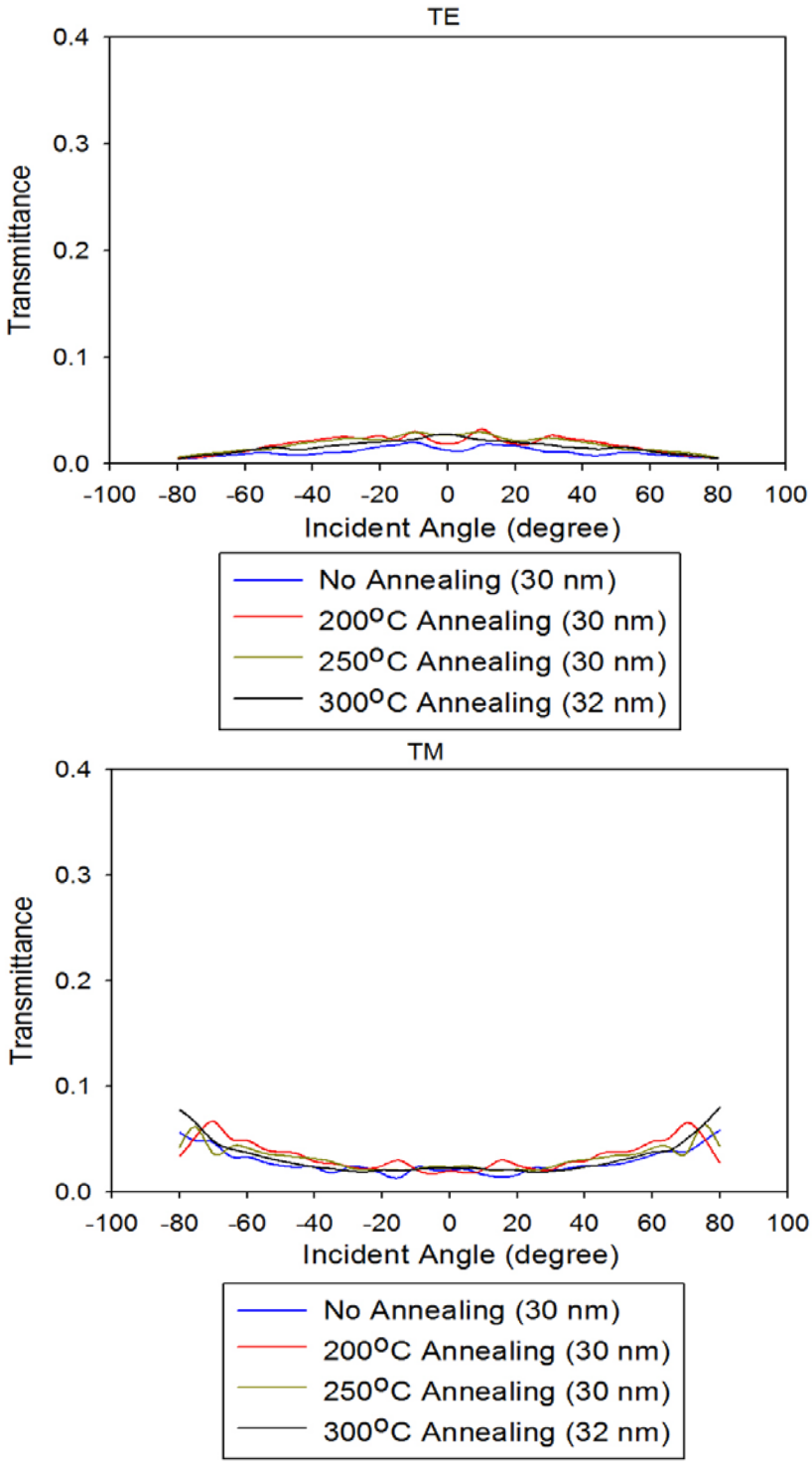

Figure 4.9 Transmittance of silver islands with 30 nm thickness at different annealing temperatures

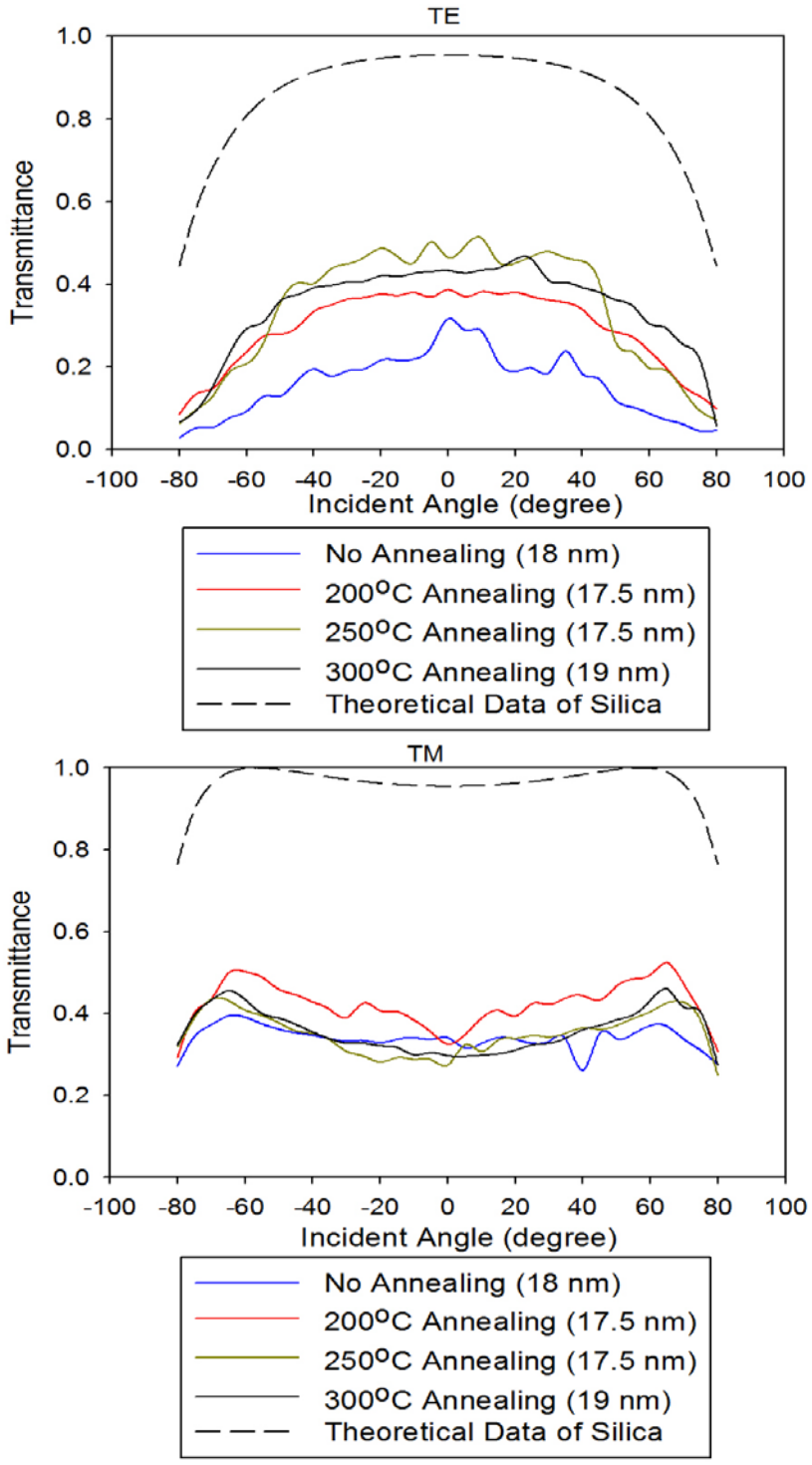

Figure 4.10 Transmittance of silver islands with 20 nm thickness at different annealing temperatures

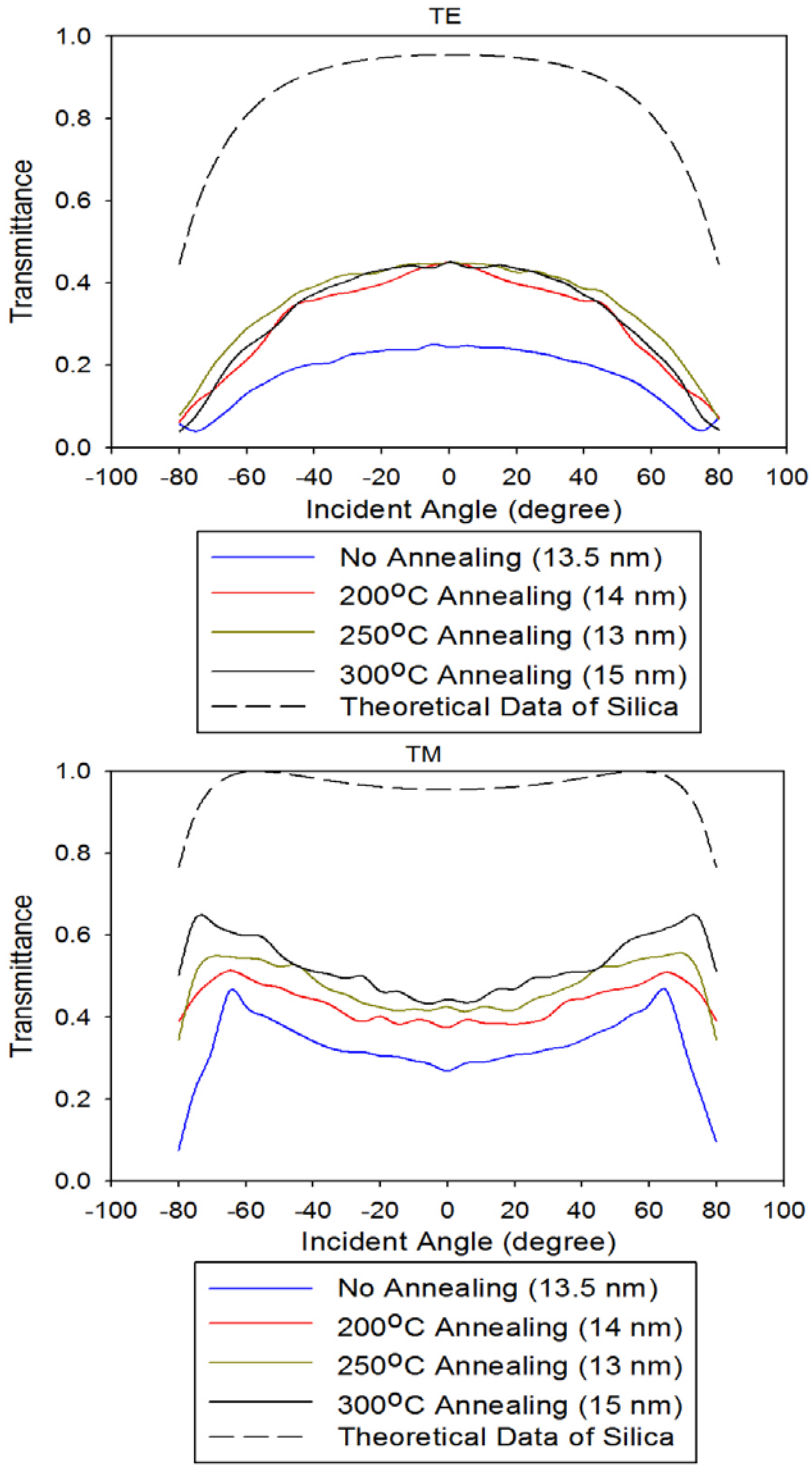

Figure 4.11 Transmittance of silver islands with 15 nm thickness at different annealing temperatures

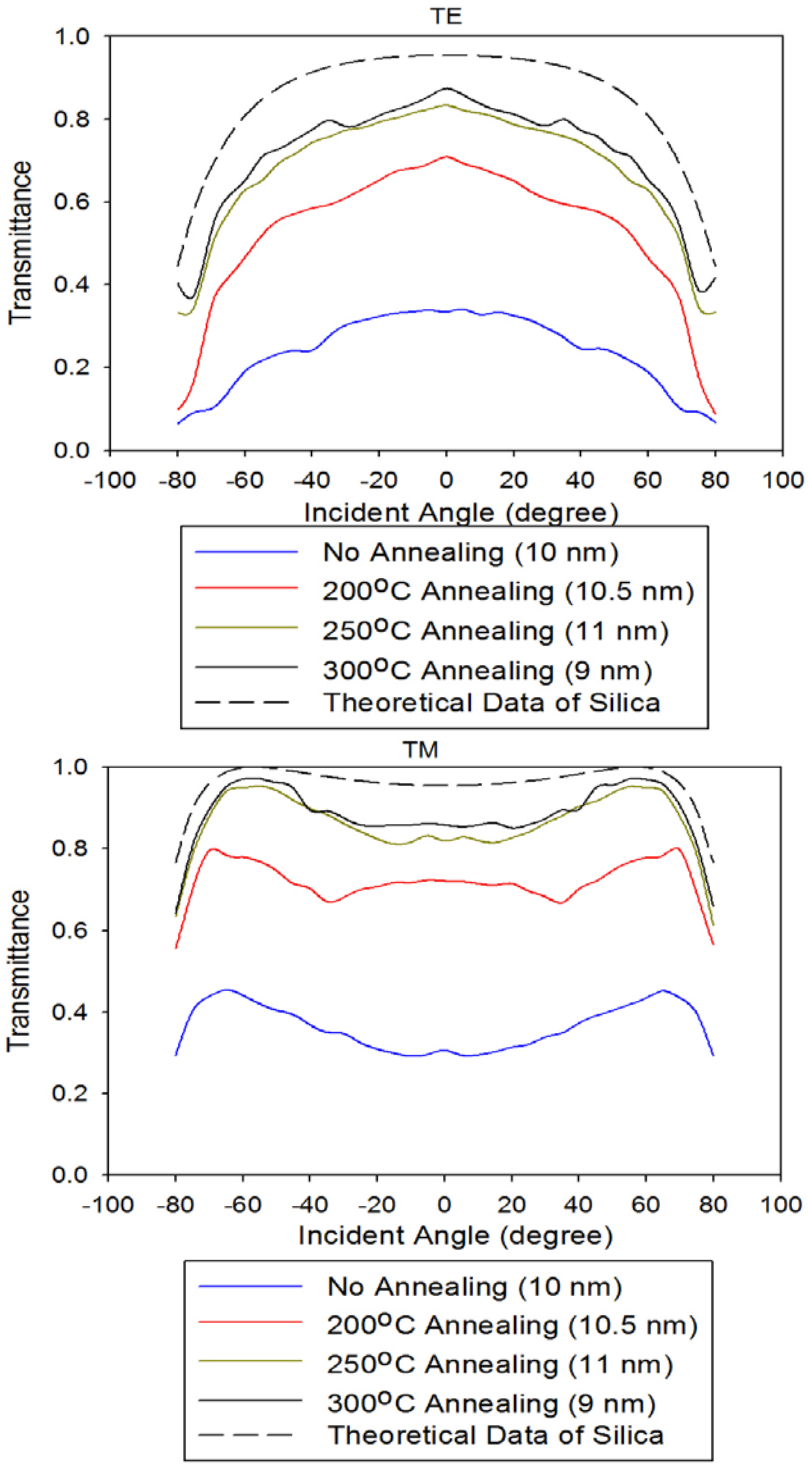

Figure 4.12 Transmittance of silver islands with 10 nm thickness at different annealing temperatures

4.2.2 Transmittance of samples with different thicknesses at the same annealing temperature

Then, from Fig. 4.13 to Fig. 4.16, the annealing temperature is fixed and we can compare results between different thicknesses. In Fig. 4.13, the transmittances of samples with 30 nm silver thickness are lower than that of samples with 20 nm silver thickness, 15 nm silver thickness and 10 nm silver thickness, while the transmittances of samples with 10 nm silver thickness are similar to that of samples with 15 nm silver thickness and 20 nm silver thickness.

However, in Fig. 4.14, the transmittance is influenced after annealing. For TE mode, the transmittance of sample with 15 nm silver thickness is similar to that of sample with 20 nm silver thickness, but the transmittance of sample with 10 nm silver thickness is higher than that of samples with either 15 nm silver thickness or 20 nm silver thickness. In other words, when the thickness is thin, the number of silver islands is few.

Even though the annealing temperature is increased, same phenomena are still observed (Fig. 4.15 and Fig. 4.16).

The difference between 15 nm silver thickness and 20 nm silver thickness can be noticed for TM mode. For TM mode, the transmittance of sample with 20 nm silver thickness is similar to that of sample with 15 nm silver thickness when the annealing temperature is 200^{o}C (Fig. 4.14). However, when the annealing temperature increases to 250^{o}C or 300^{o}C, the transmittances of samples with 20 nm silver thickness are lower than that of samples with 15 nm silver thickness for TM mode (Fig. 4.15 and Fig. 4.16). In other words, metal islands effects with 20 nm silver thickness and 15 nm silver thickness are stable when the annealing temperature is higher than 250^{o}C.

In sum, the results of the transmittance are similar to that of the reflectance. If the thickness of silver is less than 20 nm, big metal islands can be formed after annealing. However, for 20 nm silver thickness, metal islands effects are stable when the annealing temperature is higher than 250^{o}C; for 15 nm silver thickness and 10 nm silver thickness, metal islands effects are stable when the annealing temperature is higher than 200^{o}C.

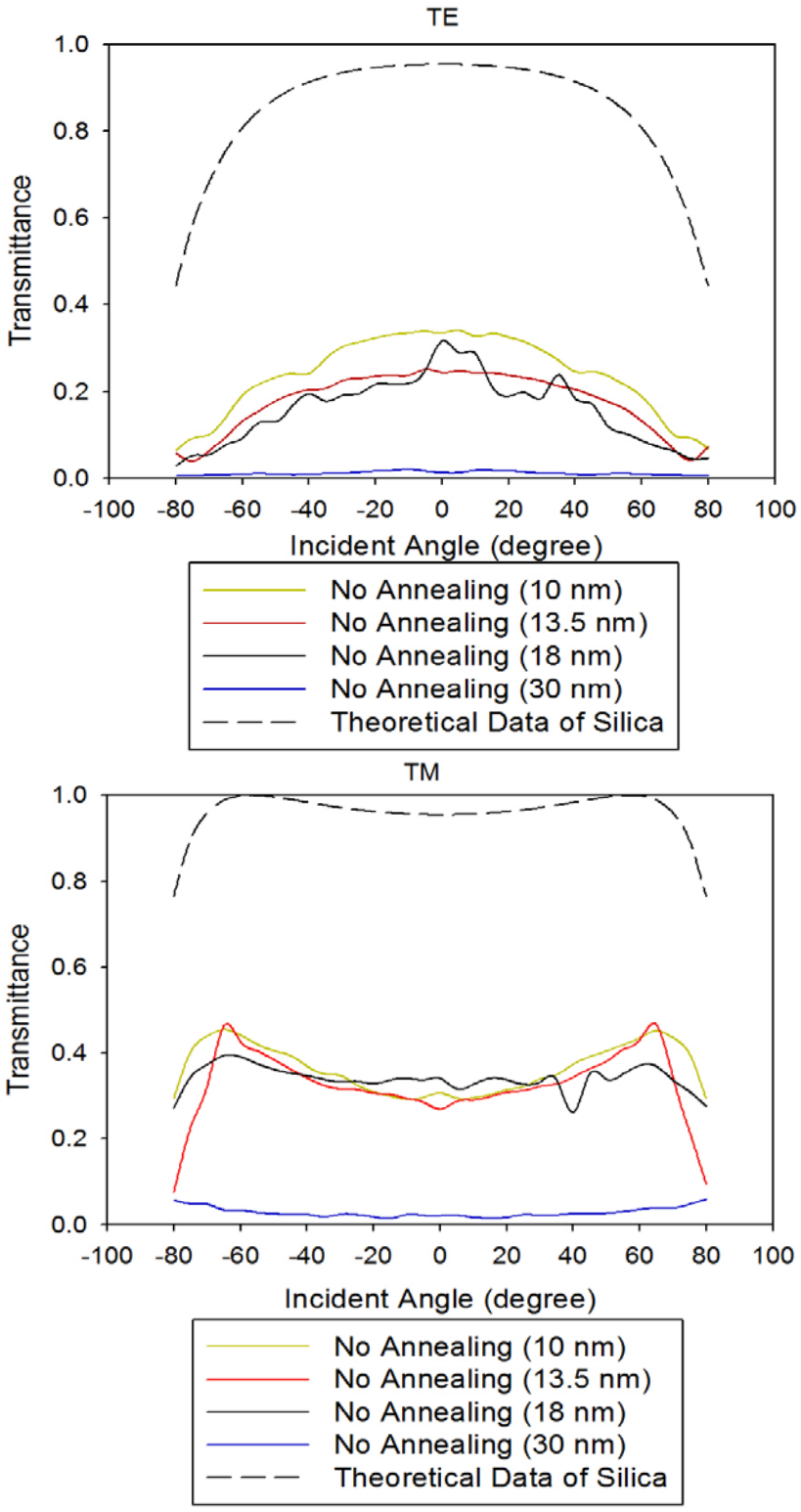

Figure 4.13 Transmittance of silver islands with different thicknesses

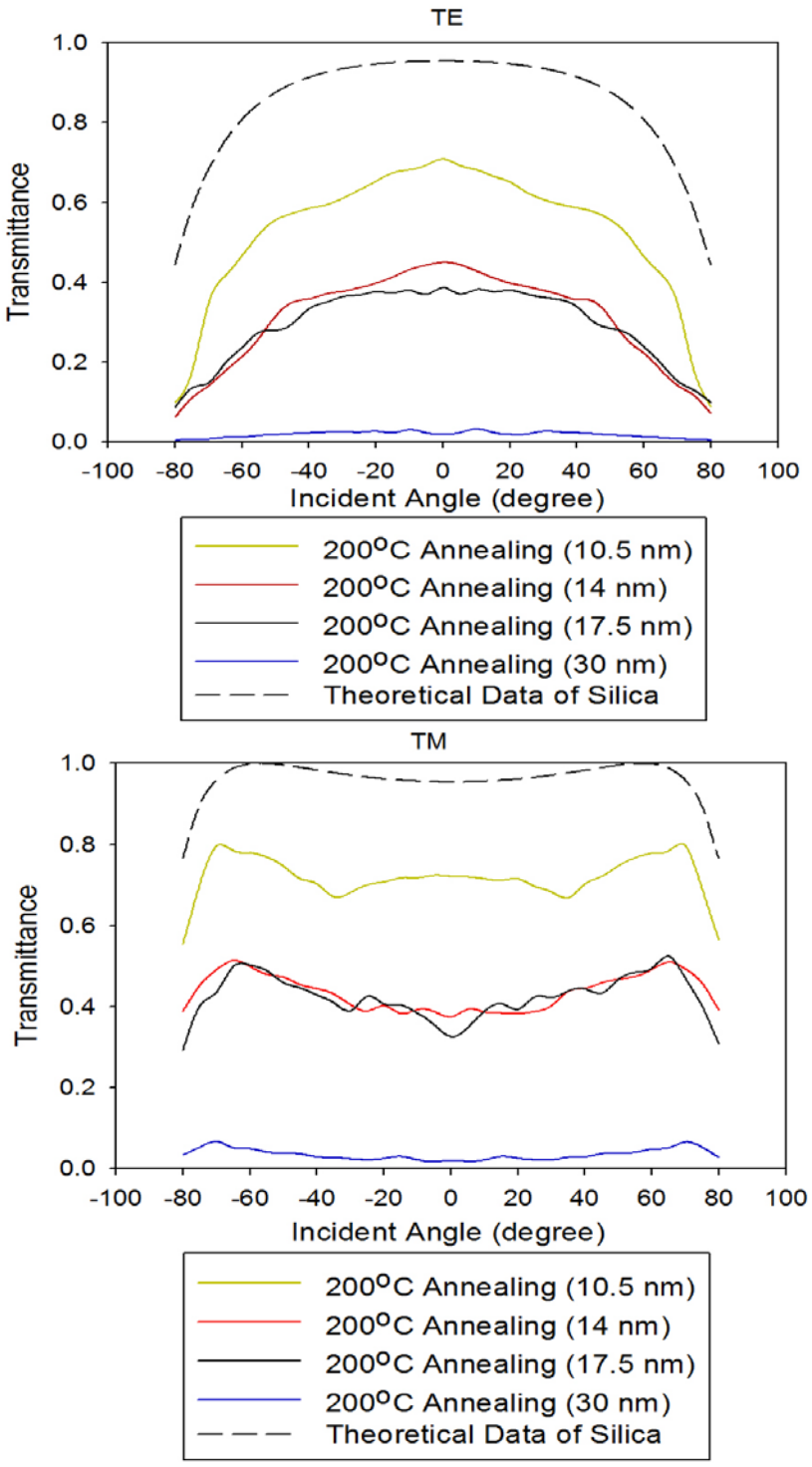

Figure 4.14 Transmittance of silver islands with different thicknesses at 200°C annealing temperature

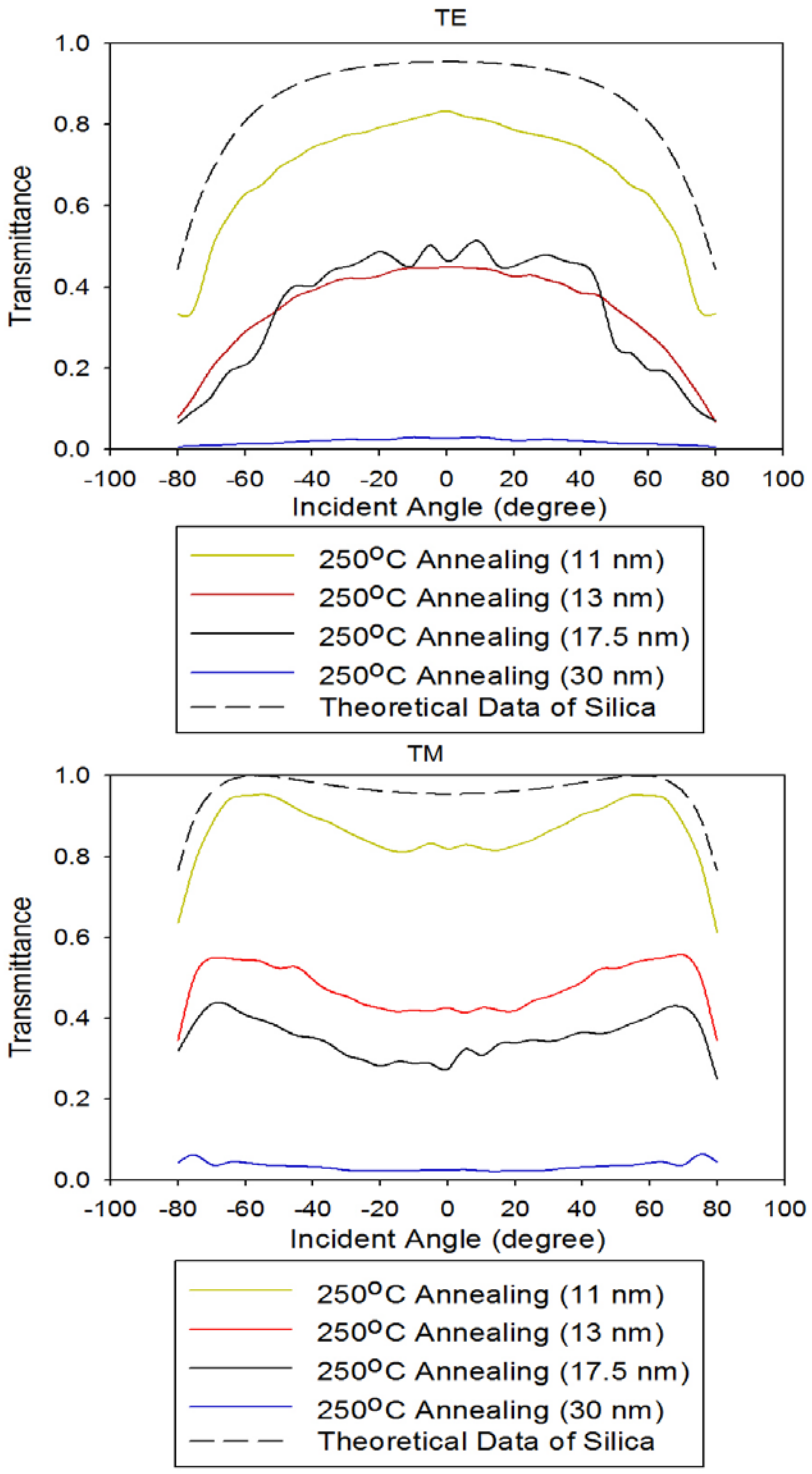

Figure 4.15 Transmittance of silver islands with different thicknesses at 250°C annealing temperature

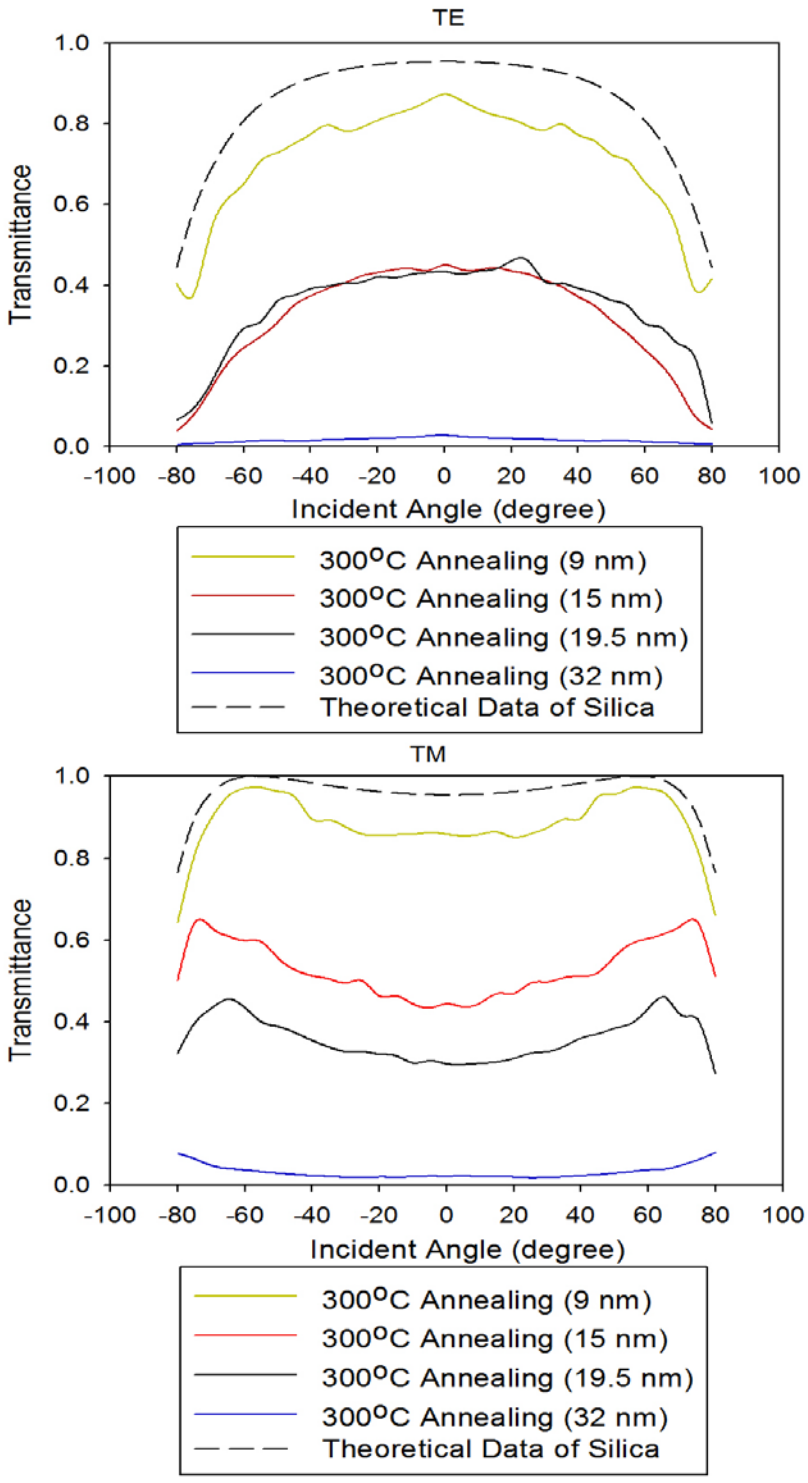

Figure 4.16 Transmittance of silver islands with different thicknesses at 300°C annealing temperature

4.3 ANALYSIS–EXTINCTION AT 633 NM WAVELENGTH

The definition of extinction is

$$\text{extinction} = 1 - \text{reflectance} - \text{transmittance} = 1 - \frac{I_R}{I_{inc}} - \frac{I_t}{I_{inc}}. \quad (4.4\text{-}1)$$

Thus, extinction can be calculated from reflectance and transmittance.

4.3.1 Extinction of samples with the same thickness at different annealing temperatures

First of all, various annealing temperatures can influence extinction via island formation. In Fig. 4.17, when the thickness of silver is 30 nm, big metal islands cannot be formed. The extinctions are very low, since the film is highly reflective.

When the thickness of silver is 20 nm, the extinctions of the annealed samples are higher than that of the un-annealed samples (Fig. 4.18). Comparing the reflectance and the transmittance, the extinction is more related to the reflectance than to the transmittance. When the thickness of silver is 20 nm, the reflectances of the un-annealed samples are always higher than that of annealed samples for both TE and TM modes as shown in Fig. 4.2. Nevertheless, the transmittance of un-annealed sample is lower than that of annealed samples for TE mode but higher than that of annealed samples for TM mode as shown in 4.10. The extinctions of the un-annealed samples are always lower than annealed samples for both modes. Thus, the extinction is much related to the reflectance when the thickness of silver is 20 nm.

In Fig. 4.19, the extinctions of the un-annealed samples are similar to that of the annealed samples when the thickness of silver is 15 nm. Because big metal islands can be formed after annealing when the thickness of silver is 20 nm, big metal islands should also be formed when

thickness of silver is 15 nm. However, the number of silver islands of the annealed samples is sparse. Even though big metal islands can be formed after annealing, the extinctions would not be influenced. In other words, the number of islands interacting with light will not be influenced by annealing. Thus, the extinctions of the annealed samples are similar to that of the un-annealed samples. Then, comparing the reflectance to the transmittance, there is no significant phenomena correlated with the extinction. Thus, the contribution of the reflectance and the transmittance to the extinction is equivalent.

In Fig. 4.20, when the thickness of silver is 10 nm, the extinctions of the annealed samples are lower than that of the un-annealed samples. Actually, after annealing, the extinctions should be elevated in regular cases. Nevertheless, the number of islands is very sparse when the thickness of silver is 10 nm. After annealing, big metal islands are formed but the number of islands interactive with light is less. Thus, the extinctions of the un-annealed samples are higher than that of the annealed samples. Then, comparing the reflectance to the transmittance, we can find that the transmittances of annealed samples are greatly elevated after annealing as shown in Fig. 4.12. According to (4.4-1), the transmittance plays a key role in the extinction since the extinctions of annealed samples are very low.

Thus, the reflectance is more important than the transmittance for the extinction when the thickness of silver is thick, but the transmittance is much important when the thickness of silver is thin.

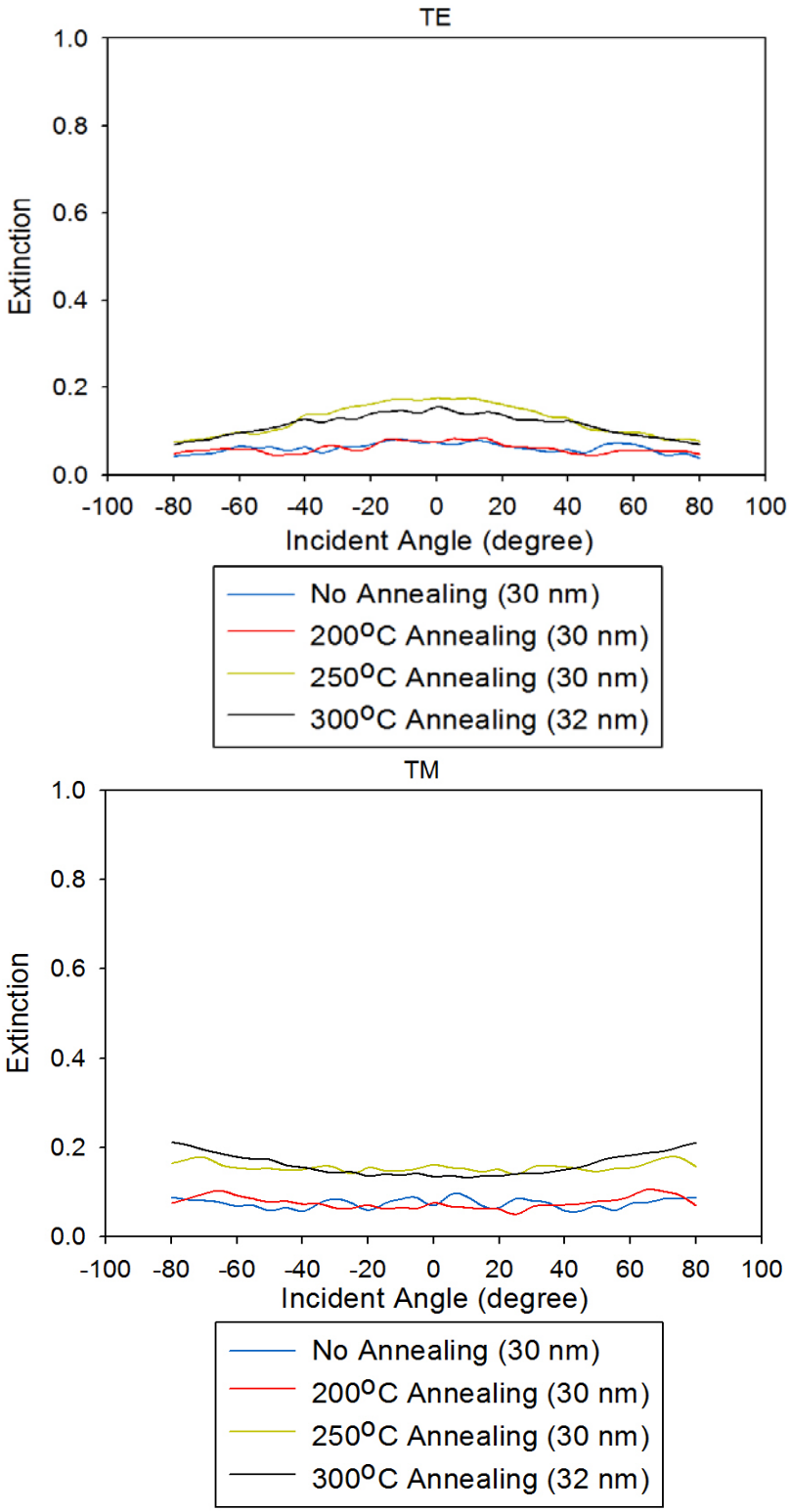

Figure 4.17 Extinction of silver islands with 30 nm thickness at different annealing temperatures

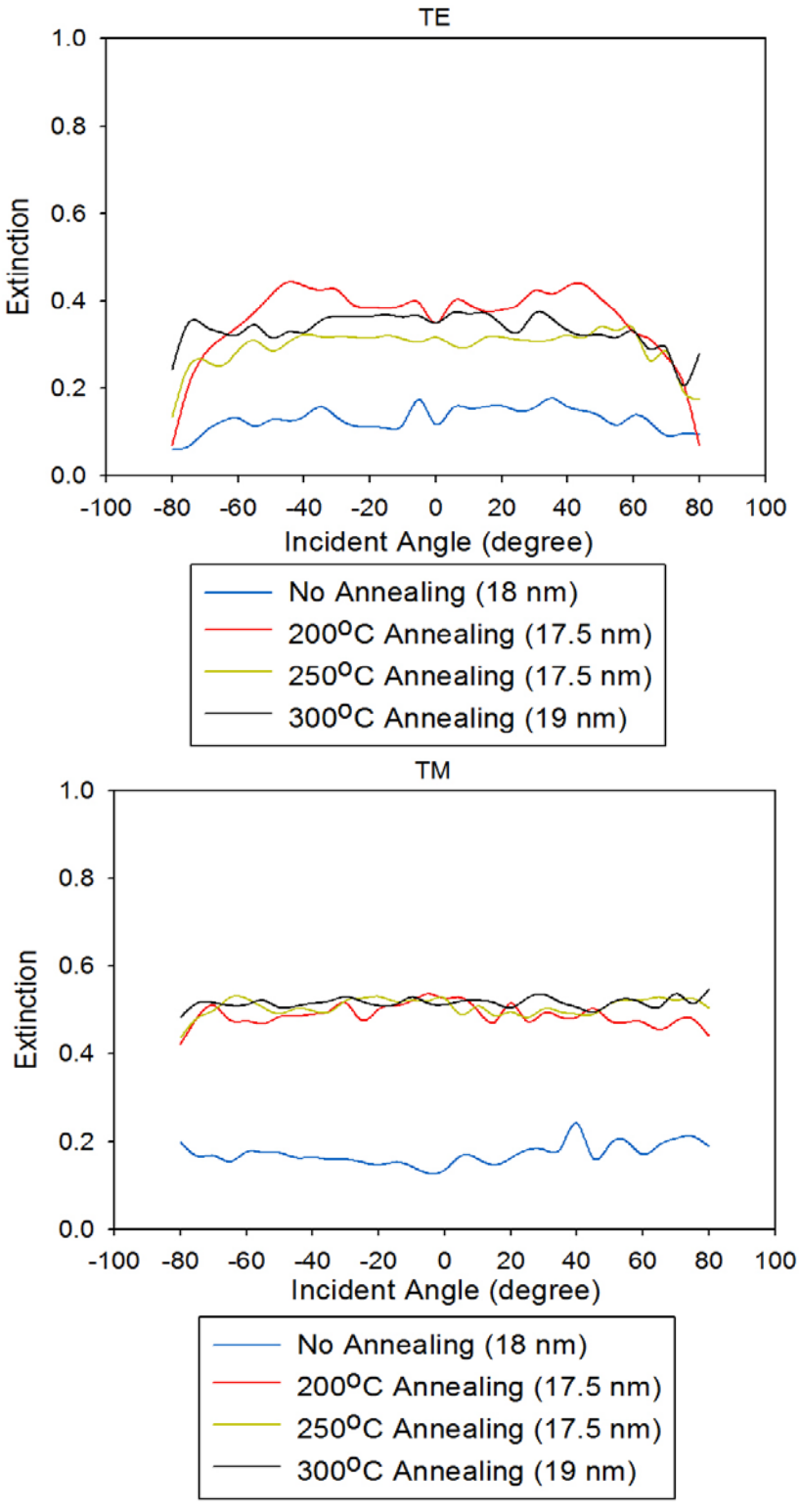

Figure 4.18 Extinction of silver islands with 20 nm thickness at different annealing temperatures

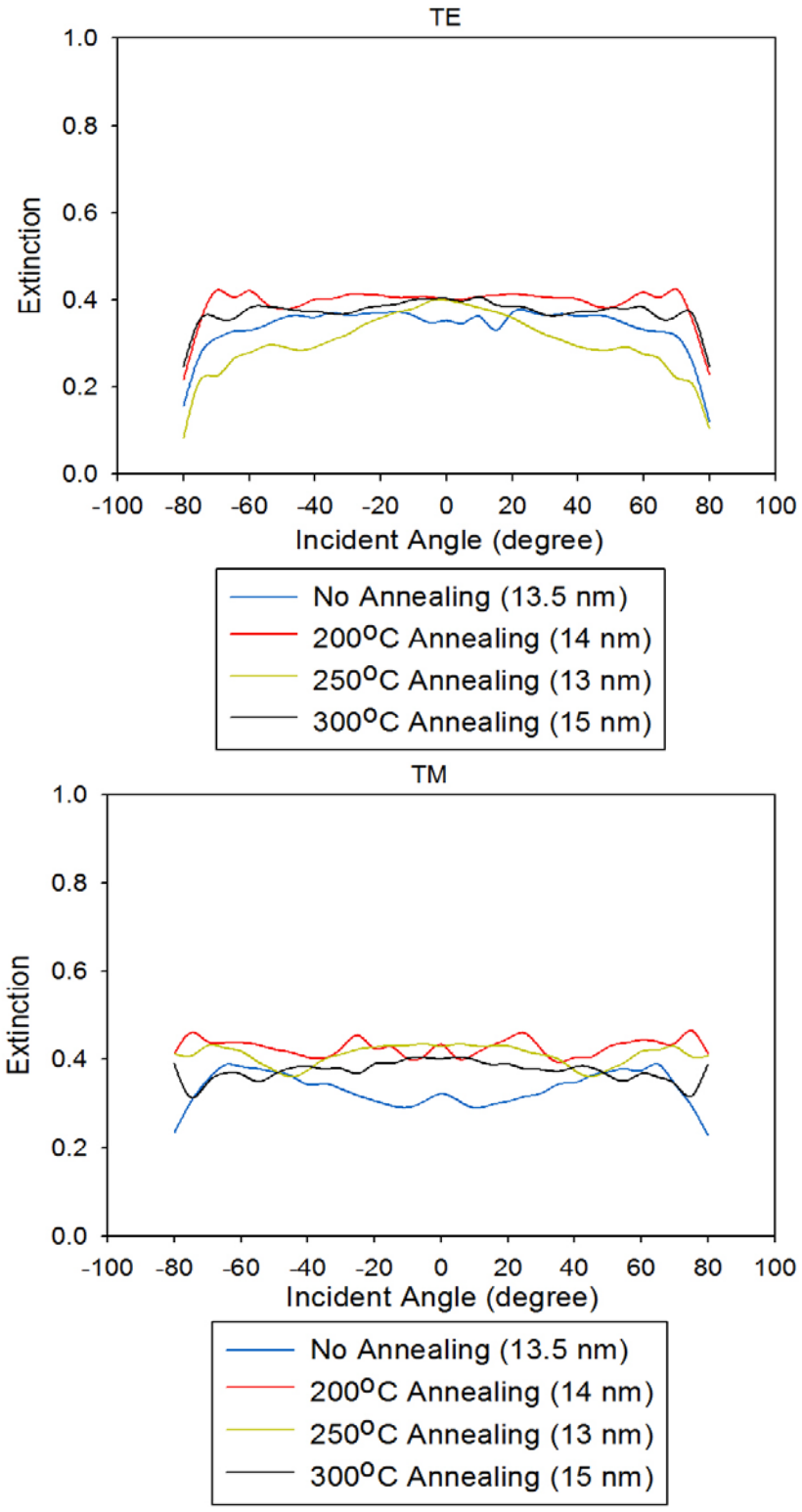

Figure 4.19 Extinction of silver islands with 15 nm thickness at different annealing temperatures

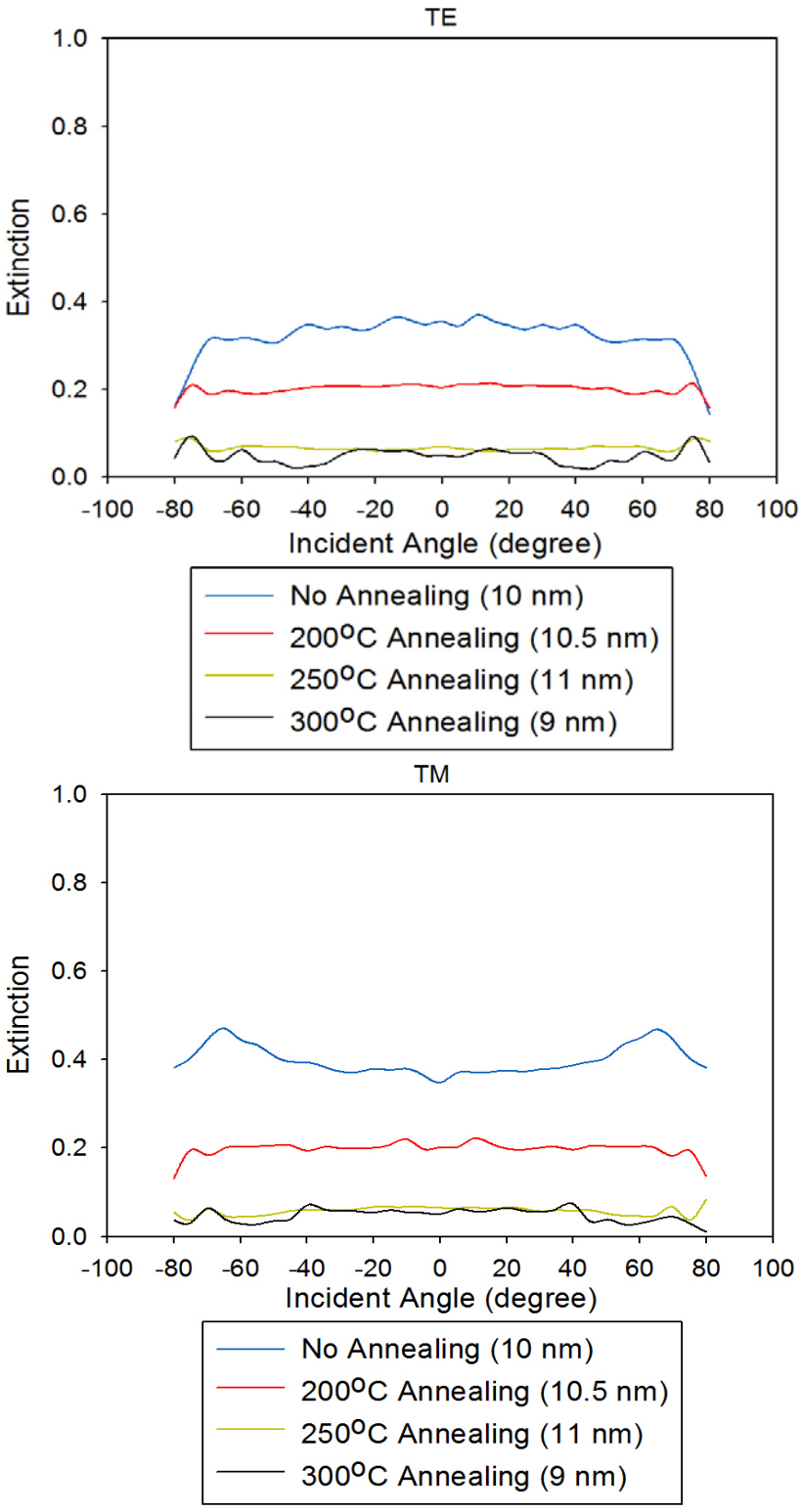

Figure 4.20 Extinction of silver islands with 10 nm thickness at different annealing temperatures

4.3.2 Extinction of samples with different thicknesses at the same annealing temperature

In Fig. 4.21, the extinctions of samples with 15 nm silver thicknesses are similar to that of samples with 10 nm silver thicknesses. In other words, the composition of silver particles with 15 nm silver thickness is similar to that with 10 nm silver thickness.

In Fig. 4.22, the extinctions of samples with 10 nm silver thickness are lower than that of samples with 15 nm silver thickness and 20 nm silver thickness since the number of silver islands is sparse. On the other hand, after annealing, the extinction of sample with 15 nm silver thicknesses is similar to that of sample with 20 nm silver thicknesses for TE mode.

Nevertheless, in Fig. 4.22 and Fig. 4.23, the difference between 20 nm silver thickness and 15 nm silver thickness is obvious for TM mode. There are two explanations for this phenomenon: First, metal islands effects are stable when the annealing temperature is higher than 200^{o}C. Second, the number of silver islands with 20 nm silver thickness is more than that with 15 nm silver thickness. One other important thing is that the extinctions of samples with 10 nm silver thicknesses are lower than that of samples with 30 nm silver thicknesses when annealing temperature is 250^{o}C as shown in Fig. 4.23, since the number of metal islands is much sparse. Fig. 4.24 showed the same phenomenon.

In sum, comparing the reflectance, the transmittance and the extinction with one another, the following results are reached. First of all, when the thickness of silver is 30 nm, the optical properties of silver are very clear. Second, when the thickness of silver is thinner than 20 nm, big metal islands can be formed after annealing. Metal islands effects with 20 nm silver thickness are stable when the annealing temperature is higher than 250^{o}C. Third, when the thickness of silver is 15 nm, metal islands effects are stable when the annealing temperature is higher than 200^{o}C

and the extinctions of the annealed samples are similar to that of the un-annealed samples. Furthermore, the number of silver islands is rare when the thickness of silver is 10 nm, and the reflectances and the extinctions are low while the transmittances are high.

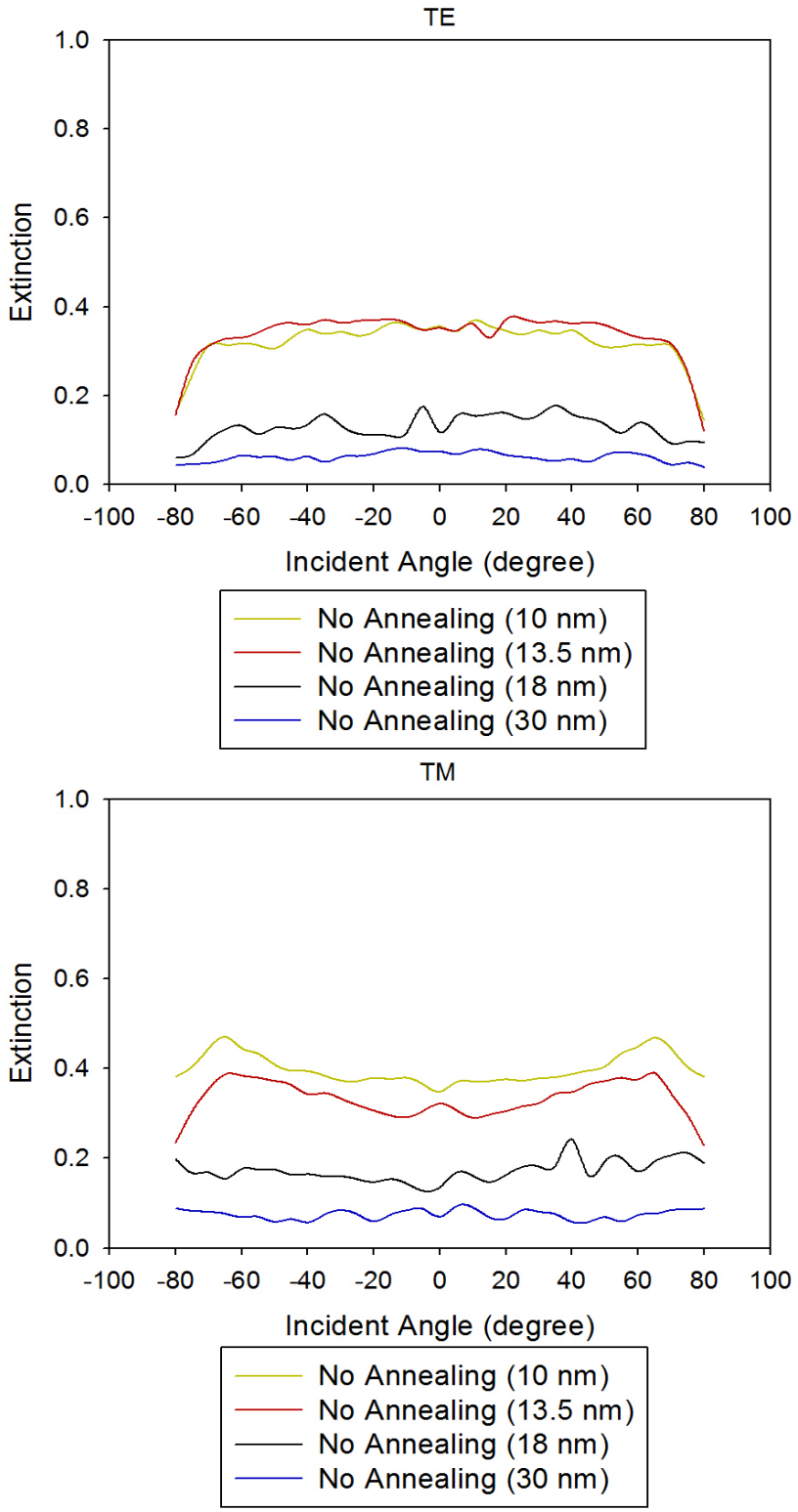

Figure 4.21 Extinction of silver islands with different thicknesses

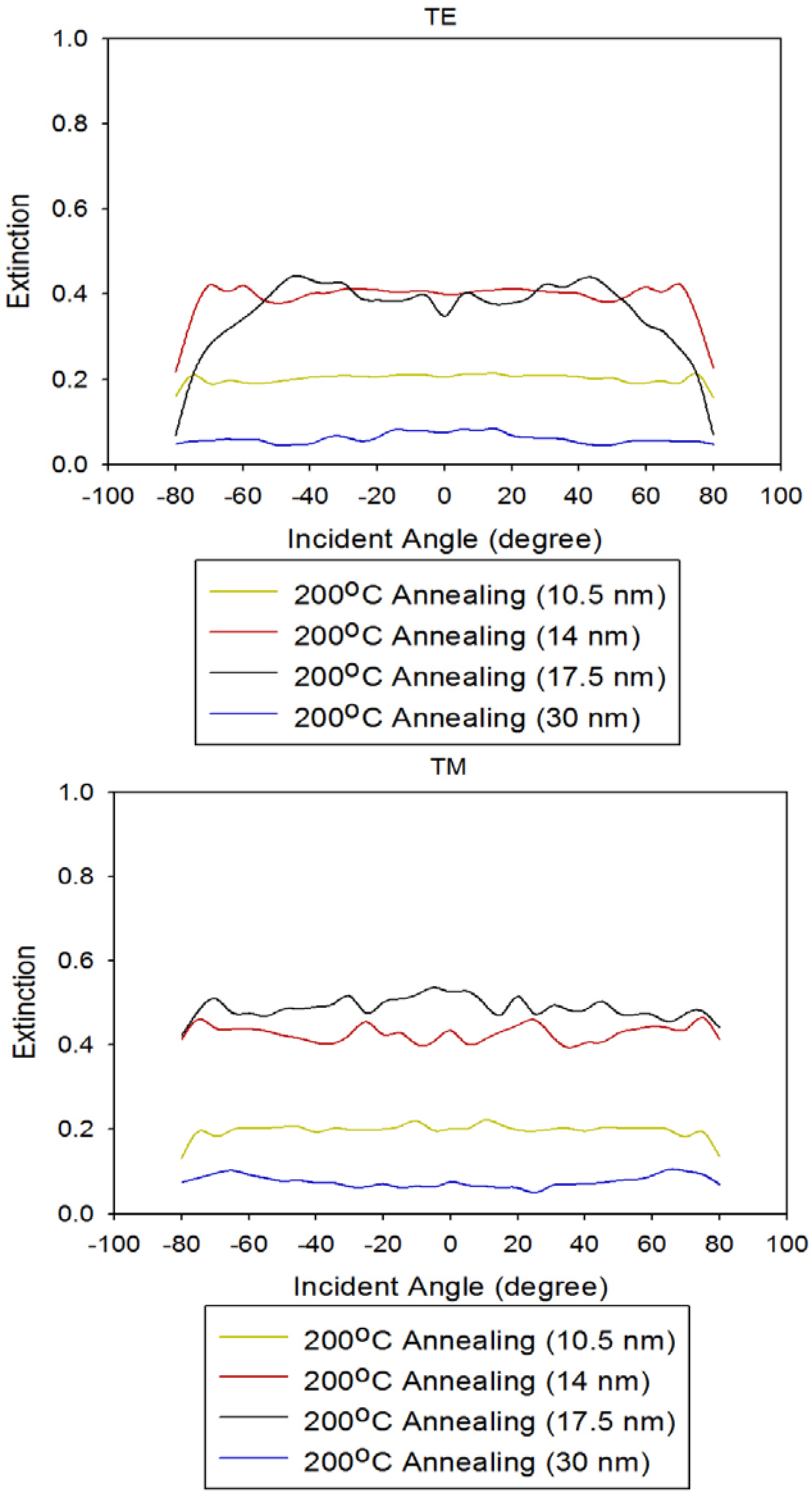

Figure 4.22 Extinction of silver islands with different thicknesses at 200°C annealing temperature

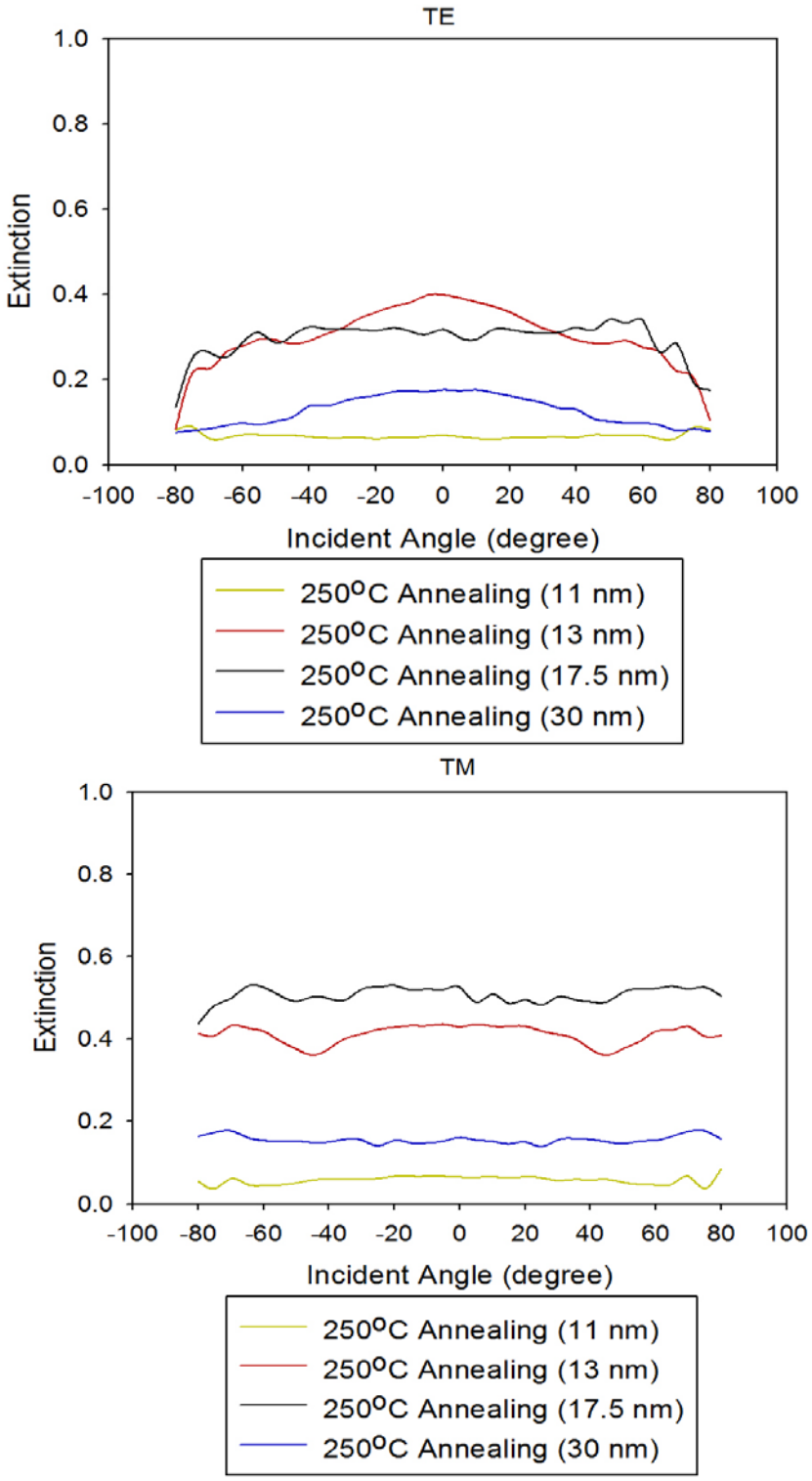

Figure 4.23 Extinction of silver islands with different thicknesses at 250°C annealing temperature

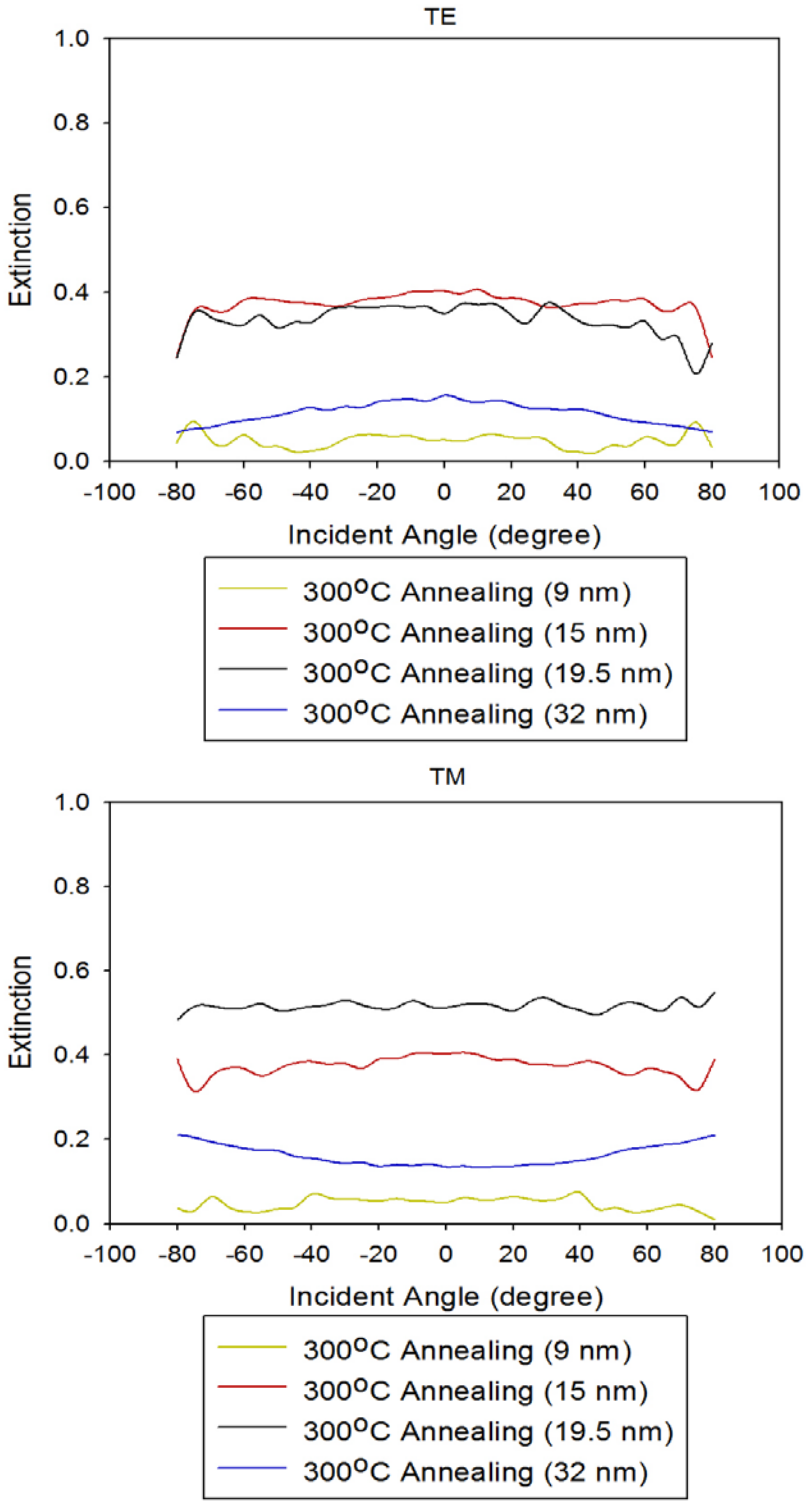

Figure 4.24 Extinction of silver islands with different thicknesses at 300°C annealing temperature

4.4 ANALYSIS–TRANSMITTANCE (WAVELENGTH: 300 NM ~ 1000 NM)

Recent study have reported [1], silver (10-27 nm thick) was deposited by thermal evaporation and was annealed at 200^{o}C. Fig. 4.25 shows the SEM figure of their samples from the same reference. According to Fig. 4.25, the average distance between two islands is (a)0.124 μm, (b)0.160 μm, (c) 0.205 μm, and (d) 0.29 μm. In our study, since we used the similar fabrication processes, the morphologies of metal islands on our samples are expected to be similar to theirs.

According to Fig. 4.25, when the silver layer is thick, the islands become big and distance between two islands is large after annealing. Meanwhile, referred to Fig 4.26(b) and Fig. 4.27, when the thickness of silver is thick, the minimum transmission points move toward long wavelength. In other words, if the thickness of silver is getting thicker, the transmission minima can move to even longer wavelength. However, in Fig. 4.28 and Fig. 4.29, the minimum transmission points are random. Fig. 4.30 shows the distance between two islands is fixed after thermal evaporation. The metal islands effects are affected by annealing, but the distance between two islands won't change. If the evaporation conditions are the same, the minimum transmission points should be at the same wavelength after annealing. In fact, our evaporation conditions are not equivalent since the silica samples were placed at different positions in the evaporation chamber. In other words, the distances between two islands are not the same. Thus, the minimum transmission points are random as shown in Fig. 4.28 and Fig. 4.29.

We also notice that the samples with 30 nm silver thickness or un-annealed samples do not show the transmission minima in the spectra. The transmission minima are correlated with the

distance between island and island. If there are no the transmission minima, the distance between two islands should be zero.

In the transmission spectra, the minimum transmission points are related with peaks since the transmission minima and the second peak appear under the same conditions. According to properties of silver, the refractive index of silver is 1.13 when wavelength of incident wave is 310 nm [19]. Referring to (2.1-15) and (2.1-16), the transmittances are 99.63% for both TE and TM modes. Thus, the first peak is correlated with the fundamental property of silver. On the other hand, the second peak should be related with surface plasmons. In the normal case,

$$\omega_p = \frac{Ne^2}{m\varepsilon} = 10^{16}\ (S^{-1}) \tag{4.4-5}$$

and

$$\lambda_p = \frac{2\pi c}{\omega_p} = 188.2\ (\text{nm}). \tag{4.4-6}$$

Since the thickness of silver is thin, the planar resonance angular frequency is correlated with silica and silver. The dielectric index of silica is 2.4. According to equation (2.3-16),

$$\omega_1 = \frac{\omega_p}{\sqrt{1+\varepsilon}} = \frac{10^{16}}{\sqrt{1+2.4}} = 5.423\times10^{15}\ (S^{-1}),\ \lambda_p = 347.6\ \text{nm}. \tag{4.4-7}$$

This value is very near the second peak as shown in Fig. 4.26 to Fig. 4.29. In Fig. 4.26 and Fig. 4.27, the second peak moves toward short wavelength when the thickness of silver is thick. On

the other hands, if there are enough silver which can interact with light and silica, the second peak is very close to theoretical value. Thus, the second peak might be planar surface resonance wavelength.

Then, we compare the transmission spectra as shown in Fig. 4.26 to Fig. 4.29.

In Fig. 4.27(a), the transmittance of sample with 30 nm silver thickness is lower than that of sample with 20 nm silver thickness, 15 nm silver thickness and 10 nm silver thickness, since the surface of sample with 30 nm silver thickness is very smooth. Moreover, the transmittance of sample with 15 nm silver thickness is similar to that of sample with 10 nm silver thickness due to the sparse number of particles and islands.

In Fig. 4.27(b), the differences between the transmittance of sample with 15 nm silver thickness and that of sample with 10 nm silver thickness is noticed. Even though the number of islands with 15 nm silver thickness is sparse, it's still more than that with 10 nm silver thickness. Thus, the transmittance of sample with 15 nm silver thickness is lower than that of sample with 10 nm silver thickness. Nevertheless, the transmittance of sample with 15 nm silver thickness is similar to that of sample with 20 nm silver thickness since metal islands effects are not obvious.

If the annealing temperature is higher than 250^{o}C, the difference between 15 nm silver thickness and 20 nm silver thickness is clear as shown in Fig. 4.28. In other words, the metal islands effects are obvious and stable when the annealing temperature is higher than 250^{o}C.

Then, we compare the transmission spectra of samples at different annealing temperatures. In Fig. 4.29(a), the transmittances of samples are always low. There are no metal islands effects.

However, in Fig. 4.29(b), a second peak is showed up and the transmittance is increased after annealing. The difference between the transmittance of samples at 250^{o}C and 300^{o}C is

small. In other words, the metal islands effects are clear and stable when the thickness is 20 nm and the annealing temperature is higher than 250^{o}C.

Same phenomena are observed in Fig. 4.30. However, the properties of silica are much obvious when thickness of silver is 10 nm. Thus, the metal islands effects should be obvious and stable when the thickness of silver is 20 nm and 15 nm, and the annealing temperature is higher than 250^{o}C.

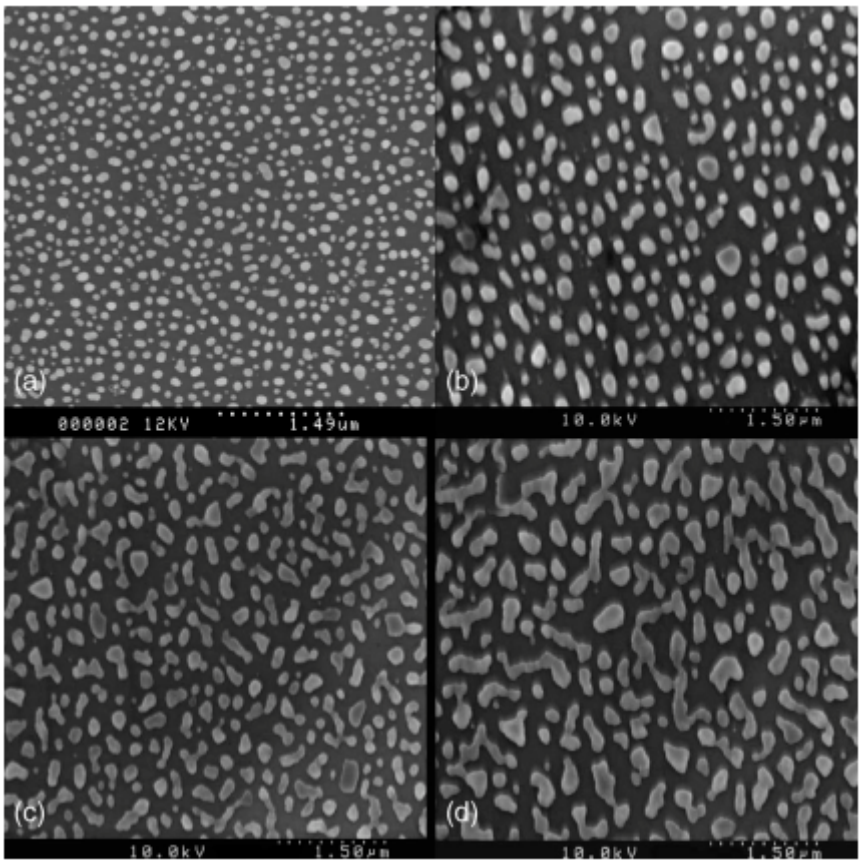

Figure 4.25 SEM pictures showing silver metal islands after annealing (a) 14 nm, (b) 16 nm, (c) 18 nm, and (d) 27 nm of silver. [Ref 1]

(a)

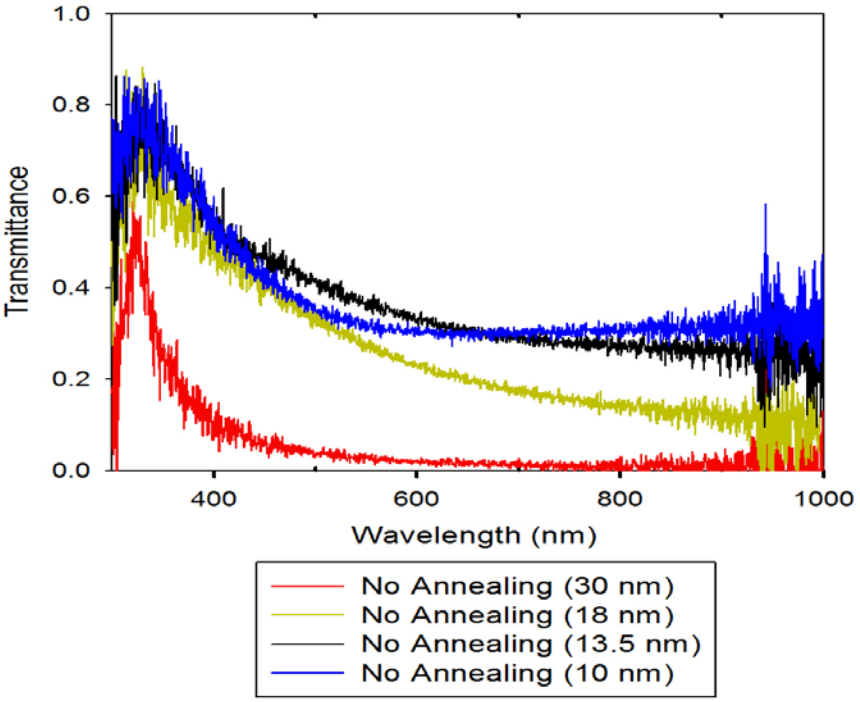

(b)

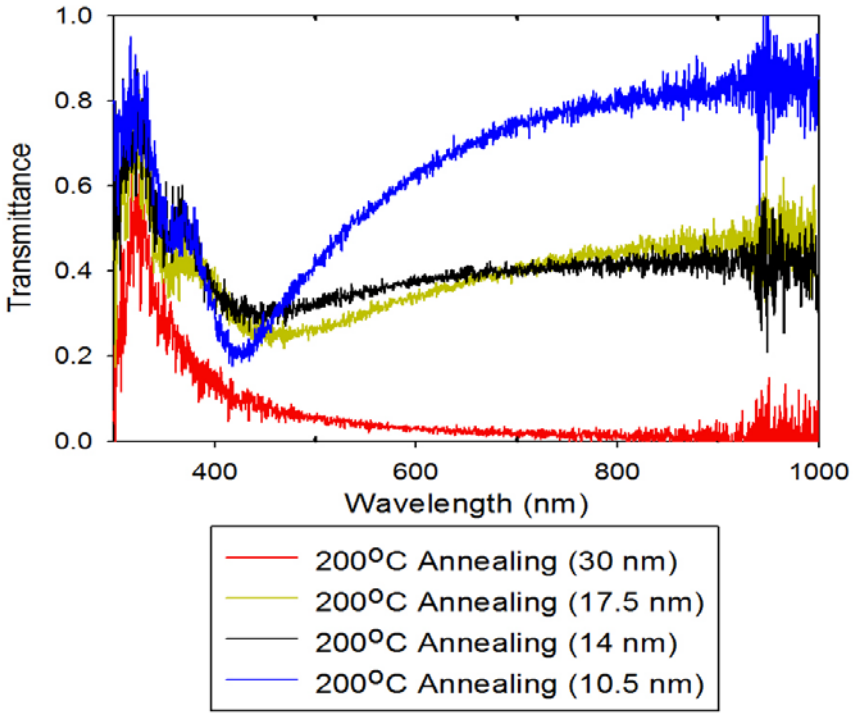

Figure 4.26 Transmission spectrum of silver islands with different thicknesses at the same annealing temperature: (a) No annealing; (b) Temperature is 200^{o}C.

(a)

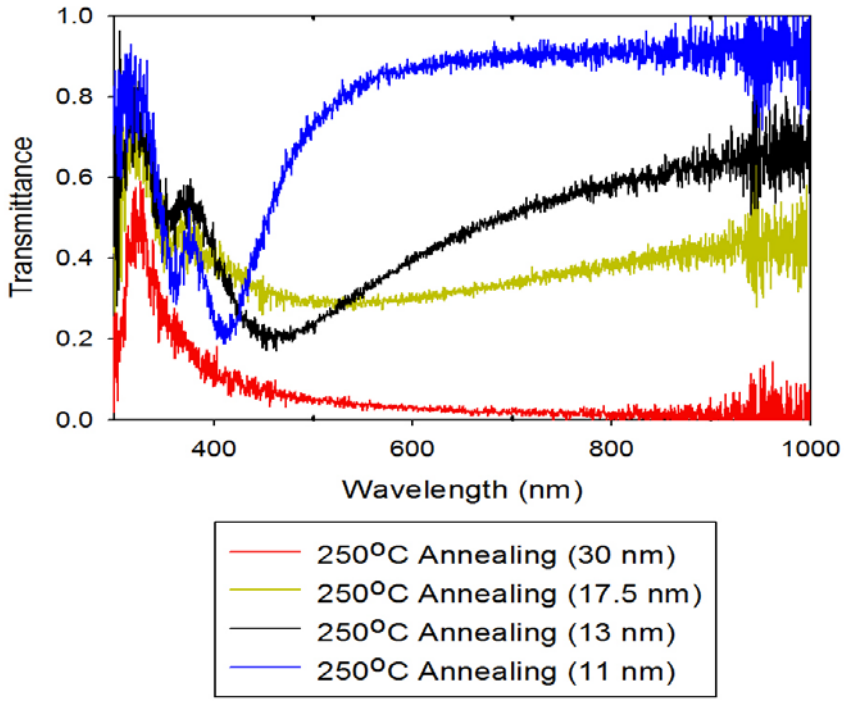

(b)

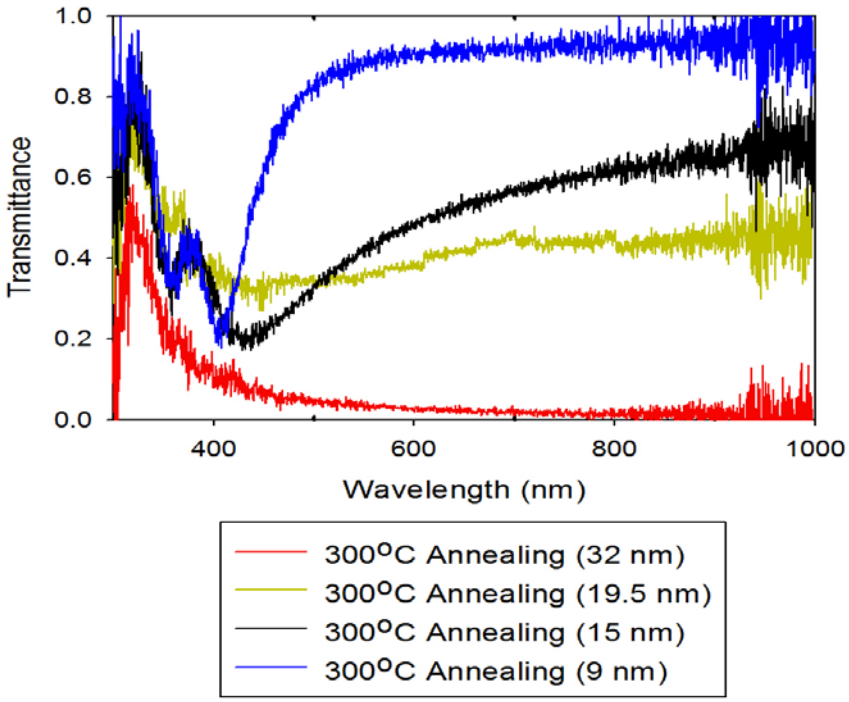

Figure 4.27 Transmission spectrum of silver islands with different thicknesses at the same annealing temperature: (a) Temperature is 250°C; (b) Temperature is 300°C.

(a)

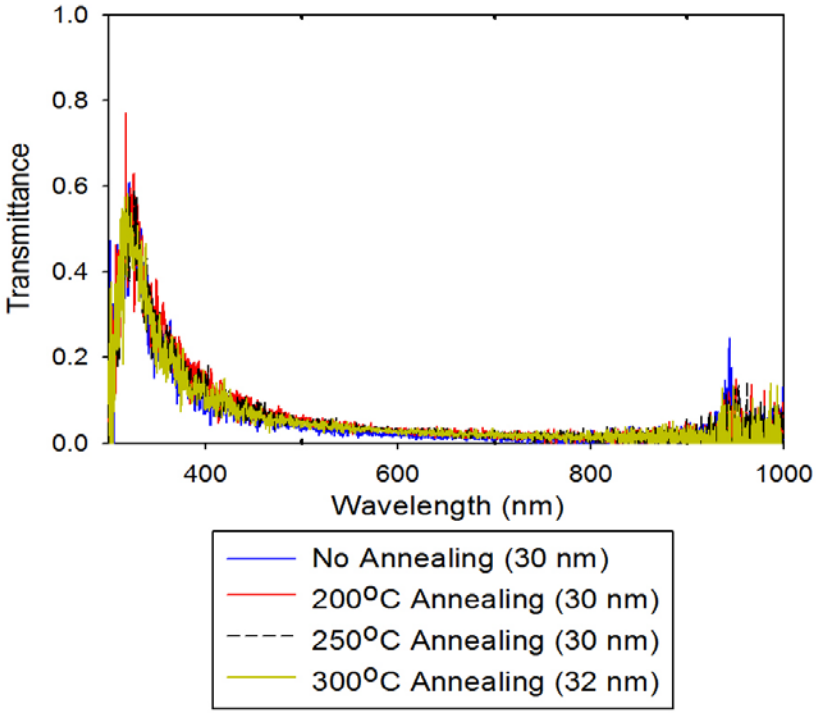

(b)

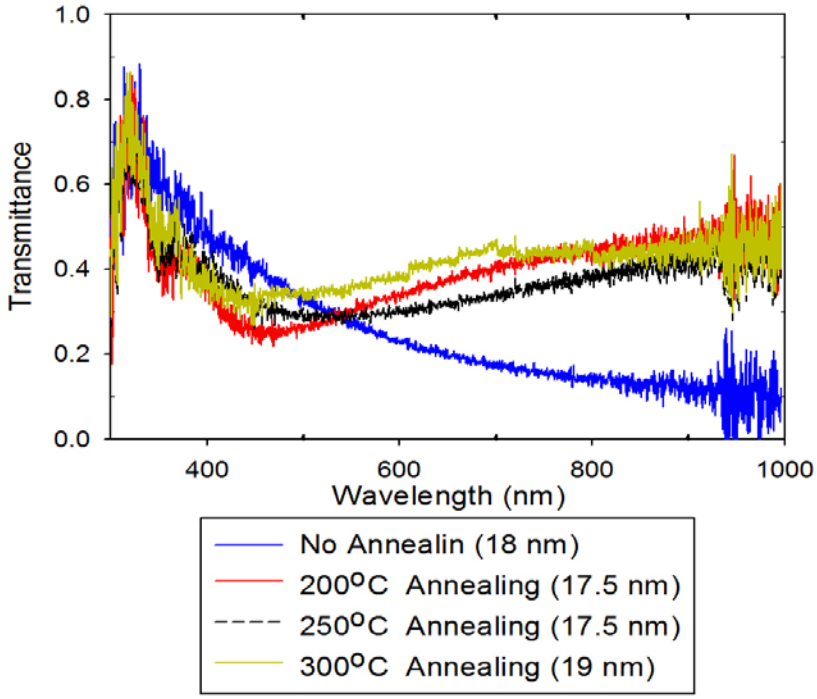

Figure 4.28 Transmission spectrum of silver islands with the same thickness at different annealing temperatures: (a) Thickness is 30 nm; (b) Thickness is 20 nm.

(a)

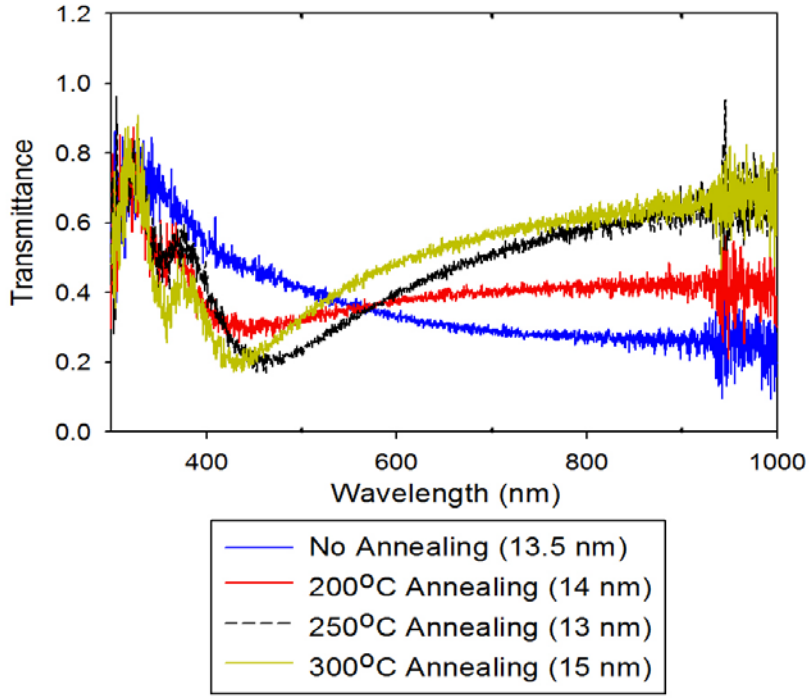

(b)

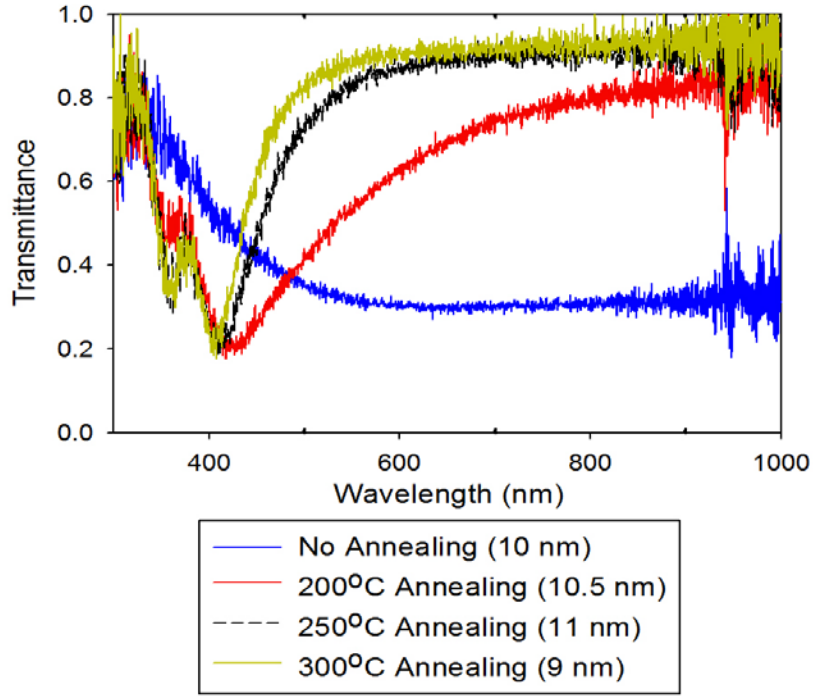

Figure 4.29 Transmission spectrum of silver islands with the same thickness at different annealing temperatures: (a) Thickness is 15 nm; (b) Thickness is 10 nm.

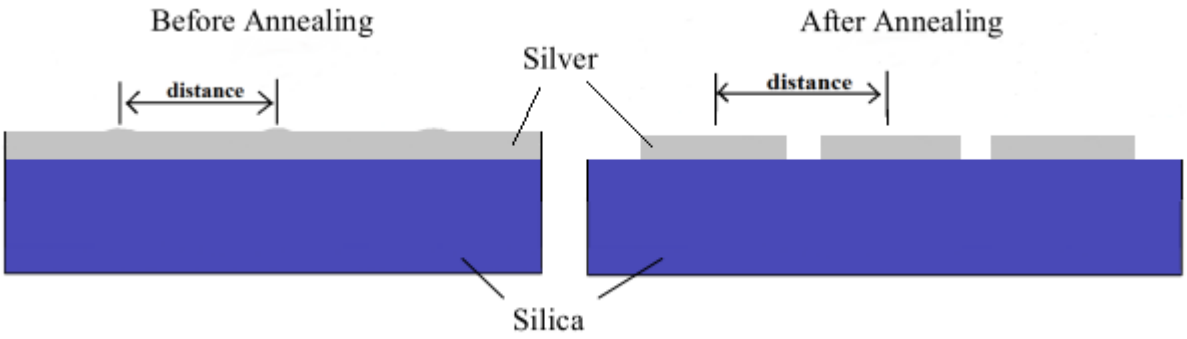

Figure 4.30 Metal islands on silica

5.0 CONCLUSION

In this study, the optical properties of silver islands on silica substrates were investigated. It is found that Ag films with 15-20 nm thickness can easily form big nano-islands upon receiving annealing ~250^{o}C. When the film thickness becomes 30 nm or greater, island formation is difficult.

Additionally, surface plasmon effects associated with metal islands are observed in the reflection/transmission spectra. Silver islands studied in this thesis might be applied to photo-voltaic devices as a means to improve trapping light

BIBLIOGRAPHY

1. S. Pillai, K. R. Catchpole, T. Trupke, and M. A. Green, “Surface plasmon enhanced silicon solar cells”, Journal of Applied Physics, 101, 093105 (2007)

2. K. R. Catchpole and S. Pillai, “Absorption enhancement due to scattering by dipoles into silicon waveguides”, Journal of Applied Physics, 100, 044504 (2006)

3. F. J. Beck, A. Polman, and K. R. Catchpole, “Tunable light trapping for solar cells using localized surface plasmons”, Journal of Applied Physics, 105, 114310 (2009)

4. Harry A. Atwater and Albert Polman, “ Plasmonics for improved photovoltaic devices”, Nature Materials, VOL 9, 205-214 (March 2010)

5. Howard R. Stuart and Dennis G. Hall, “Absorption enhancement in silicon-on-insulator waveguides using metal island films”, Appl. Phys. Lett. 69 (16), 2327-2329 (October 1996)

6. Howard R. Stuart and Dennis G. Hall, “Island size effects in nanoparticle-enhanced photodetectors”, Appl. Phys. Lett., Vol. 73, No. 26, 3815-3817 (December 1998)

7. Kazutaka Baba, Toshiaki Okuno, and Mitsunobu Miyagi, “Silver-gold compound metal island films prepared by using a two-step evaporation method”, Appl. Phys. Lett. 62 (5), 437-439 (February 1993)

8. Howard R. Stuart and Dennis G. Hall, “Enhanced Dipole-Dipole Interaction between Elementary Radiators Near a Surface”, Physical Review Letters, VOL 80, Number 25, 5663-5666 (JUNE 1998)

9. A.L. Stepanov, D.E. Hole, “Reduction of the size of the implanted silver nanoparticles in float glass during excimer laser annealing”, Applied Surface Science 136 , 298-305, (1998)

10. A. Yariv and P. Yeh, “Photonics”, Oxford, 66-232 (2007)

11. P. Yeh, “Optical Waves in Layered Media”, JOHN WILEY & SONS, 37-82 (2005)

12. Heinz Raether, “Surface Plasmons on Smooth and Rough Surfaces and on Gratings”, Springer-Verlag, 4-39 (1998)

13. Takayuki Okamoto, “Near-Field Spectral Analysis of Metallic Beads”, Appl. Phys. 81, 97–123 (2001)

14. Jenny Nelson, “Physics of Solar Cells”, Imperial College Press, 79-323 (2010)

15. Royer, J.P. Gpudonnet and R.J. Warmack, “Substrate effects on surface-plasmon spectra in metal-island films”, Phys. Rev. B 35, 3753–3759, (1987)

16. S. H. Lim, W. Mar, P. Matheu, D. Derkacs, and E. T. Yu, “Photocurrent spectroscopy of optical absorption enhancement in silicon photodiodes via scattering from surface plasmon polaritons in gold nanoparticles”, J. Appl. Phys. **101**, 104309, (2007)

17. U. Kreibig and M. Vollmer, “Optical Properties of Metal Clusters”, Springer, 13-41 (1995)

18. Zhijun Sun, Yun Suk Jung, and Hong Koo Kim, “ Role of Surface Plasmons in the Optical Interaction in Metallic Gratings with Narrow Slits”, Applied Physics Letters, VOL 83, Number 15, 3021-3023 (October 2003)

19. P. B. Johnson and R. W. Christy, “Optical Constants of the Noble Metals”, Physical Review B, VOL 6, Number 12, 4370-4379 (1972)